bioRxiv preprint doi: https://doi.org/10.1101/077743; this version posted September 27, 2016. The copyright holder for this preprint (which was not certified by peer review) is the author/funder. All rights reserved. No reuse allowed without permission.

# CO-OPERATION, COMPETITION AND CROWDING: A DISCRETE FRAMEWORK LINKING ALLEE KINETICS, NONLINEAR DIFFUSION, SHOCKS AND SHARP-FRONTED TRAVELLING WAVES

STUART T. JOHNSTON[1,2], RUTH E. BAKER[3], D.L SEAN MCELWAIN[1,2], AND MATTHEW J. SIMPSON[*1,2]

Abstract. Invasion processes are ubiquitous throughout cell biology and ecology. During invasion, individuals can become isolated from the bulk population and behave differently. We present a discrete, exclusion-based process that models the birth, death and movement of individuals. The model distinguishes between individuals that are part of, or are isolated from, the bulk population by imposing different rates of birth, death and movement. This enables the simulation of various co-operative or competitive mechanisms, where there is a positive or negative benefit associated with being part of the bulk population, respectively. The mean-field approximation of the discrete process gives rise to 22 different classes of partial differential equation, which include Allee kinetics and nonlinear diffusion. Here we examine the ability of each class of partial differential equation to support travelling wave solutions and interpret the long time behaviour in terms of the individual-level parameters. For the first time we show that the strong Allee effect and nonlinear diffusion can result in shock-fronted travelling waves. We also demonstrate how differences in group and individual motility rates can influence the persistence of a population and provide conditions for the successful invasion of a population.

## Introduction

Processes where individuals invade, and subsequently colonise, a region of space are prevalent in cell biology and ecology [1–11]. In cell biology, wound healing involves the invasion of fibroblasts into the wound space for tissue regeneration [7]. The invasion of glioma cells throughout the brain can lead to the formation of malignant brain tumours (glioblastoma) [1, 3, 10]. In ecology, the introduction and subsequent invasion of an alien species is a significant factor contributing

* Corresponding author: Matthew J. Simpson (matthew.simpson@qut.edu.au).
[1]Mathematical Sciences, Queensland University of Technology (QUT), Brisbane, Australia.
[2]Tissue Repair and Regeneration Program, Institute of Health and Biomedical Innovation, QUT, Brisbane, Australia.
[3]Wolfson Centre for Mathematical Biology, Mathematical Institute, University of Oxford, United Kingdom.

bioRxiv preprint doi: https://doi.org/10.1101/077743; this version posted September 27, 2016. The copyright holder for this preprint (which was not certified by peer review) is the author/funder. All rights reserved. No reuse allowed without permission.



to the extinction of native species [2, 11].

During invasion, individuals that become separated from the bulk population have been observed to have different behaviours to individuals within the bulk population [8, 12–15]. This is intuitive in ecological processes, as a decrease in the number of individuals within the bulk population can reduce the number of potential mates [13, 15–17] or lessen the efficacy of predator avoidance [14–16]. In cell biology, individual micrometastases have been observed to have growth thresholds, which suggests that the presence of additional cells enhances the birth rate [12].

Continuum mathematical models of invasion processes have been studied extensively since the Fisher-Kolmogorov model was first proposed in 1937 [15, 18–30]. The Fisher-Kolmogorov model is a partial differential equation (PDE) description of the evolution of population density, where the temporal change in population density at a point is attributed to a combination of linear diffusion and logistic growth [24, 27]. The Fisher-Kolmogorov model has been applied to various problems in cell biology and ecology [31–34]. The logistic growth term implies that the population density will always tend toward the carrying capacity [29]. This prediction does not reflect the observation that isolated individuals can experience a reduction in their birth rate [14]. This effect, known as the Allee effect, has two known forms. First, the strong Allee effect, where the growth rate is negative for sufficiently low densities [15, 35]. Second, the weak Allee effect, where the growth rate is reduced, but remains positive, at low densities [15]. Reaction-diffusion PDEs incorporating linear diffusion and Allee growth kinetics have been proposed and analysed [15, 19, 22, 23, 25, 26, 28, 30]. A key feature of interest for models of invasion is whether the PDE supports a travelling wave solution, where a wave front of constant shape moves through space with a constant speed. The sign of the wave speed indicates whether successful invasion occurs, and the magnitude of the wave speed provides an estimate of how quickly a population invades or recedes. More complicated descriptions with either Fisher or Allee kinetics and density-dependent nonlinear diffusion have been proposed, with the motivation of describing spatial aggregation or segregation [36–41].

A key feature of the Fisher-Kolmogorov model, and many extensions thereof, is that these PDE models are typically derived using phenomenologically-based arguments without incorporating information from an underlying stochastic description of individual-level behaviours. In this work

bioRxiv preprint doi: https://doi.org/10.1101/077743; this version posted September 27, 2016. The copyright holder for this preprint (which was not certified by peer review) is the author/funder. All rights reserved. No reuse allowed without permission.



we consider a relatively straightforward lattice-based discrete birth-death-movement model. An important characteristic of the model is that it explicitly accounts for crowding effects by only allowing for one agent per lattice site. Additionally, the rates at which birth, death and movement events occur depend on whether an agent is part of a group of agents or is isolated. We demonstrate that the standard continuum approximation of this discrete model can lead to either logistic or Allee kinetics, in an appropriate parameter regime. Furthermore, we demonstrate that imposing a different motility rate for agents that are isolated, compared to other agents, leads to a variety of density-dependent nonlinear diffusion mechanisms. Previous studies have examined many different types of phenomenologically-based PDEs that are motivated in an ad hoc fashion. In contrast, our PDE description arises from a single, relatively simple, physically-motivated model. In Table 1 we highlight this generality, as the single discrete model gives rise to 22 different classes of PDE that describe the population-level behaviour.

While several of these PDEs have been studied previously, for completeness we examine the ability of each class of PDE to support travelling wave solutions. For certain classes of PDE, we present details of the travelling wave solutions for the first time. Interestingly, we obtain travelling wave solutions for PDEs that have nonlinear diffusivity functions with regions of negative diffusivity. Furthermore, we show that the strong Allee effect combined with these diffusivity functions can lead to novel shock-fronted travelling wave solutions. As these diffusivity functions are obtained directly from a discrete model, we can determine which competitive/co-operative individual-level mechanisms result in shock-fronted travelling wave solutions. Similarly, we are able to interpret the influence of motility on the persistence of a population, and highlight how this influence varies nonlinearly with the carrying capacity density. More generally, we provide new insight into the long time behaviour of an invasive population in terms of the individual-level properties.

bioRxiv preprint doi: https://doi.org/10.1101/077743; this version posted September 27, 2016. The copyright holder for this preprint (which was not certified by peer review) is the author/funder. All rights reserved. No reuse allowed without permission.



| | Nonlinear diffusivity | Degenerate diffusivity | Number of non-degenerate zeros | Negative diffusivity | Source Term | Grouped agent death | Relevant previous analysis |
|---|---|---|---|---|---|---|---|
| Case 1 | x | x | 0 | x | Fisher | x | [18–21, 24, 25, 27, 29] |
| Case 2: Sub-case 1 | ✓ | x | 0 | x | Fisher | x | [42–44] |
| Case 2: Sub-case 2 | ✓ | ✓ | 0 | x | Fisher | x | [40, 45–47] |
| Case 2: Sub-case 3 | ✓ | x | 2 | ✓ | Fisher | x | [36] |
| Case 2: Sub-case 4 | ✓ | ✓ | 1 | ✓ | Fisher | x | [38] |
| Case 3 | x | x | 0 | x | Fisher | ✓ | [18–21, 24, 25, 27] |
| Case 4: Sub-case 1 | ✓ | x | 0 | x | Fisher | ✓ | [42–44] |
| Case 4: Sub-case 2 | ✓ | ✓ | 0 | x | Fisher | ✓ | [40, 45–47] |
| Case 4: Sub-case 3 | ✓ | x | 2 | ✓ | Fisher | ✓ | [36] |
| Case 4: Sub-case 4 | ✓ | ✓ | 1 | ✓ | Fisher | ✓ | [38] |
| Case 4: Sub-case 5 | ✓ | x | 1 | ✓ | Fisher | ✓ | [38] |
| Case 5 | x | x | 0 | x | Allee | x | [15, 19, 22, 23, 25, 26, 28, 30] |
| Case 6: Sub-case 1 | ✓ | x | 0 | x | Allee | x | [45, 48] |
| Case 6: Sub-case 2 | ✓ | ✓ | 0 | x | Allee | x | [41, 49] |
| Case 6: Sub-case 3 | ✓ | x | 2 | ✓ | Allee | x | [37] |
| Case 6: Sub-case 4 | ✓ | ✓ | 1 | ✓ | Allee | x | [39] |
| Case 7 | x | x | 0 | x | Allee | ✓ | [15, 19, 22, 23, 25, 26, 28, 30] |
| Case 8: Sub-case 1 | ✓ | x | 0 | x | Allee | ✓ | [45, 48] |
| Case 8: Sub-case 2 | ✓ | ✓ | 0 | x | Allee | ✓ | [41, 49] |
| Case 8: Sub-case 3 | ✓ | x | 2 | ✓ | Allee | ✓ | [37] |
| Case 8: Sub-case 4 | ✓ | ✓ | 1 | ✓ | Allee | ✓ | [39] |
| Case 8: Sub-case 5 | ✓ | x | 1 | ✓ | Allee | ✓ | [39] |

TABLE 1. **Different classes of PDE associated with the discrete model in appropriate parameter regimes**. An Allee source term can correspond to either the weak, strong or reverse Allee effect. Degenerate diffusivity refers to the case where $F(C^*) = R(C^*) = 0$ for some value $C^*$.

bioRxiv preprint doi: https://doi.org/10.1101/077743; this version posted September 27, 2016. The copyright holder for this preprint (which was not certified by peer review) is the author/funder. All rights reserved. No reuse allowed without permission.



## Results

We consider a discrete lattice-based exclusion process where agents undergo birth, death and movement events. We distinguish between isolated agents and grouped agents by imposing different rates of birth, death and movement depending on whether an agent has zero or at least one nearest-neighbour agent, respectively. The corresponding PDE description of this process is

$$\frac{\partial C}{\partial t} = \frac{\partial}{\partial x}\left(F(C)\frac{\partial C}{\partial x}\right) + R(C), \tag{1}$$

where

$$F(C) = D_i(1 - 4C + 3C^2) + D_g(4C - 3C^2),$$
$$R(C) = \lambda_g C(1 - C) + (\lambda_i - \lambda_g - K_i + K_g)C(1 - C)^2 - K_g C,$$

$C(x, t)$ is the agent density, $D_i$ and $D_g$ are the diffusivities, $\lambda_i$ and $\lambda_g$ describe the birth rates, and $K_i$ and $K_g$ describe the death rates for isolated and grouped agents, respectively. Full details of the discrete process, the corresponding PDE, and the relationship between the discrete and continuum parameters are presented in the Methods. Equation (1) can be applied on an arbitrary one-dimensional domain, with a range of boundary conditions and initial conditions. These details are discussed later when specific solutions of Equation (1) are presented and analysed.

The aims of this work are to first illustrate that the very different types of behaviour encoded in the discrete model are also reflected in the solution of Equation (1). Once we have demonstrated this connection, we focus on examining travelling wave solutions for the 22 different classes embedded within Equation (1), as summarised in Table 1.

Twenty identically-prepared realisations of the discrete model are presented in Figures 1(a)-(f) for two different parameter regimes. In the first parameter regime, where $P_d^g = 0$, the initially-occupied region of the lattice remains fully occupied, as shown in Figures 1(a)-(c). When we introduce $P_d^g > 0$, as shown in Figures 1(d)-(f), the initially-occupied region of the lattice becomes partially vacant as time increases. We also compare the average discrete behaviour and the corresponding numerical solution of Equation (1) in Figures 1(g)-(h). This comparison shows that the solution of the continuum PDE matches the average discrete behaviour well, and predicts both the spread of the agent population in Figure 1(g) and the decrease in agent density

bioRxiv preprint doi: https://doi.org/10.1101/077743; this version posted September 27, 2016. The copyright holder for this preprint (which was not certified by peer review) is the author/funder. All rights reserved. No reuse allowed without permission.



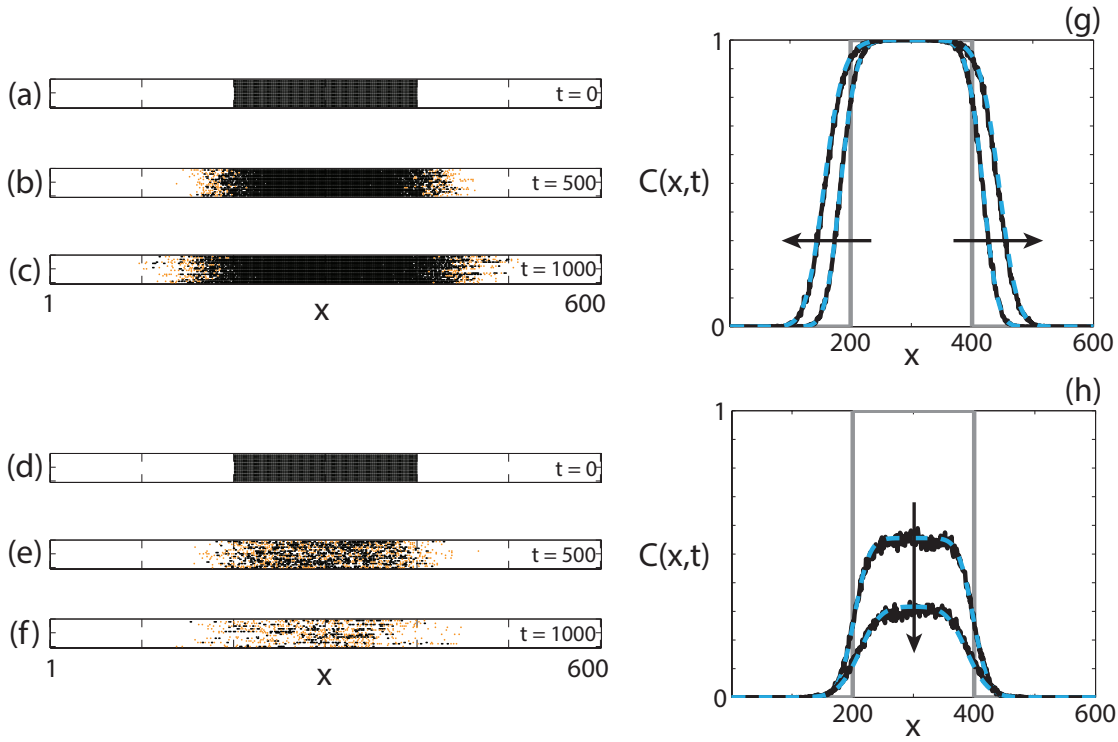


FIGURE 1. **Comparison of the discrete model and the continuum approximation**. (a)-(f) 20 identically-prepared realisations of the discrete model at (a), (d) $t = 0$, (b), (e) $t = 500$, (c), (f) $t = 1000$. The discrete model simulations correspond to (a)-(c) $P_m^i = P_m^g = 1$, $P_p^i = P_p^g = 0.005$, $P_d^i = 0.002$, $P_d^g = 0$ and (d)-(f) $P_m^i = P_m^g = 1$, $P_p^i = P_p^g = 0.005$, $P_d^i = 0.008$, $P_d^g = 0.002$. For all simulations $\tau = 1$, $\Delta = 1$. (g)-(h) Comparisons between the averaged discrete model (black, solid) and the numerical solution of Equation (1) (cyan, dashed) at $t = 0$, $t = 500$ and $t = 1000$ for the parameters in (a)-(c) and (d)-(f), respectively. The grey lines indicate the initial condition and the arrow indicates the direction of increasing time. For all discrete solutions, $M = 1000$, $X = 600$, $\Delta = \tau = 1$. For all continuum solutions, $\delta x = 1$, $\delta t = 0.1$, $\epsilon = 10^{-6}$.

in Figure 1(h).

The governing PDE, Equation (1), can be simplified in specific parameter regimes. While several of these simplified PDEs have been studied extensively, we summarise all non-trivial cases here for completeness. It is instructive to consider each case and discuss the implications of the long term behaviour in terms of the discrete model parameters, as previous derivations of these PDEs have arisen from a variety of ad hoc arguments rather than working with a single unifying model.

bioRxiv preprint doi: https://doi.org/10.1101/077743; this version posted September 27, 2016. The copyright holder for this preprint (which was not certified by peer review) is the author/funder. All rights reserved. No reuse allowed without permission.



In Table 1 we summarise the salient features of 22 different special cases of Equation (1). The nonlinear diffusivity function, $F(C)$, has four key properties:

- $F(C)$ can either be a constant, or a function of the density of individuals;
- $F(C)$ can be degenerate, which implies that at one or more densities, $C^*$, we have $F(C^*) = R(C^*) = 0$;
- $F(C)$ can be zero at values of $C^*$ that are non-degenerate, that is, $F(C^*) = 0,\ R(C^*) \neq 0$. In our model, this can occur at either zero, one or two different values of $C$; and
- $F(C)$ can be negative for an interval of $C$ values.

The source term, $R(C)$, has two key properties:

- $R(C)$ can represent either Fisher kinetics (logistic growth) or Allee kinetics (bistable); and
- the grouped agent death rate, $P_d^g$, can be zero or non-zero. If the rate is non-zero, the carrying capacity density is reduced.

There are three different types of Allee kinetics considered in this work; weak, strong and reverse. We combine these three kinetics for brevity, as it is relatively simple to change the parameter regime to alter the type of Allee effect, without changing the competitive/co-operative mechanism described. The reverse Allee effect, which we describe here for the first time, refers to a growth rate that is reduced at high density, compared to logistic kinetics, but remains positive.

Eight cases of different combinations of co-operative, competitive or neutral mechanisms are now considered systematically. Some of these cases involve distinct sub-cases so that, in total, we consider 22 different classes of PDE models of invasion.

**Case 1: Equal motility rates, equal proliferation rates, no agent death.** For $P_m^i = P_m^g$, $P_p^i = P_p^g$ and $P_d^i = P_d^g = 0$, there is no co-operative or competitive mechanism. This gives $F(C) = D = D_i = D_g$, and $R(C) = \lambda C(1-C)$, where $\lambda = \lambda_i = \lambda_g$. Therefore, Equation (1) reduces to the Fisher-Kolmogorov equation [24, 27, 29]

$$\frac{\partial C}{\partial t} = D\frac{\partial^2 C}{\partial x^2} + \lambda C(1-C). \tag{2}$$

bioRxiv preprint doi: https://doi.org/10.1101/077743; this version posted September 27, 2016. The copyright holder for this preprint (which was not certified by peer review) is the author/funder. All rights reserved. No reuse allowed without permission.



As the source term is non-negative for all physical values of $C \geq 0$, the agent population will always eventually reach the carrying capacity.

The Fisher-Kolmogorov equation has been studied extensively [18–21, 24, 25, 27, 29]. Here we present the key results in the context of examining the long time travelling wave solution. We seek right moving travelling waves in the co-ordinate $z = x - vt$, $-\infty < z < \infty$, where $v$ is a constant wave speed [29]. Transforming Equation (2) into the travelling wave co-ordinate gives

$$D\frac{\mathrm{d}^2C}{\mathrm{d}z^2} + v\frac{\mathrm{d}C}{\mathrm{d}z} + \lambda C(1-C) = 0, \quad -\infty < z < \infty. \tag{3}$$

With $U = \mathrm{d}C/\mathrm{d}z$, Equation (3) can be expressed as a system of ordinary differential equations (ODEs),

$$\frac{\mathrm{d}C}{\mathrm{d}z} = U, \tag{4}$$

$$\frac{\mathrm{d}U}{\mathrm{d}z} = -\frac{v}{D}U - \frac{\lambda}{D}C(1-C). \tag{5}$$

This system has two equilibrium points: $(C, U) = (0, 0)$, and $(C, U) = (1, 0)$. The linear stability of these equilibrium points can be analysed by examining the eigenvalues of the Jacobian at each equilibrium point. At $(0, 0)$ the characteristic equation has solutions $\xi = (-v \pm \sqrt{v^2 - 4\lambda D})/2D$, implying that $(0, 0)$ is a stable node provided that $v > 2\sqrt{\lambda D}$, and a stable spiral (focus) otherwise, as $\lambda$ and $D$ are both positive. We therefore have a minimum wave speed condition, $v^* = 2\sqrt{\lambda D}$, that must be satisfied otherwise the solution trajectory will enter non-physical regions of the phase plane [29]. The Jacobian of the linearised system at $(1, 0)$ has eigenvalues $\xi = (-v \pm \sqrt{v^2 + 4\lambda D})/2D$, implying that $(1, 0)$ is a saddle point.

The phase plane and associated heteroclinic orbit for Equations (4)-(5) are shown in Figure 2(a). Details of the numerical techniques used to solve Equation (3) and to generate the phase planes are given in the Methods. Provided $v \geq 2\sqrt{\lambda D}$ we observe a heteroclinic orbit between $(1, 0)$ and $(0, 0)$. The numerical solution of Equation (3) and the numerical solution of Equation (2), transformed into $(C, U)$ co-ordinates, are superimposed, showing a good match. This result is unsurprising, as Equation (3) is solved using the minimum wave speed, $v = v^* = 2\sqrt{\lambda D}$, and the numerical solution of Equation (2) evolves from a Heaviside initial condition, which is known to approach a travelling wave moving at the minimum wave speed [29]. The numerical solution of Equation (2) at $t = 25$ and $t = 50$ is shown in Figure 2(b), confirming that the waveform does

bioRxiv preprint doi: https://doi.org/10.1101/077743; this version posted September 27, 2016. The copyright holder for this preprint (which was not certified by peer review) is the author/funder. All rights reserved. No reuse allowed without permission.



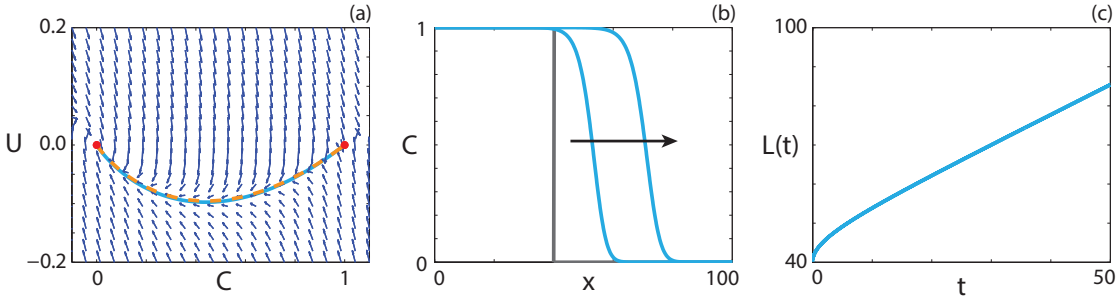


FIGURE 2. **Travelling wave behaviour for the Fisher-Kolmogorov model (Case 1).** (a) Phase plane for the system (4)-(5). Red circles denote equilibrium points. The numerical solutions of Equation (2) (cyan, solid) and Equation (3) (orange, dashed), in $(C, U)$ co-ordinates, are superimposed. (b) Numerical solution of Equation (2) at $t = 25$ and $t = 50$ (blue). The grey line indicates the initial condition and the arrow indicates the direction of increasing time. (c) The time evolution of $L(t)$. All results are obtained using $P_m^i = P_m^g = 1$, $P_p^i = P_p^g = 0.3$, $P_d^g = P_d^i = 0$, $\delta x = 0.1$, $\delta t = 0.01$, $\epsilon = 10^{-6}$, $v = 0.768$.

not change with time. To quantify the wave speed we calculate the time evolution of the leading edge, $L(t) = x_f$ such that $C(x_f, t) \approx 1 \times 10^{-4}$. If the solution of Equation (2) forms a travelling wave, $L(t)$ will tend to a straight line with slope $v$, as $t \to \infty$. In Figure 2(c), we observe that $L(t)$ is approximately linear with slope $v$, and hence the solution of Equation (2) moves with approximately constant speed at late time. Overall, these features suggest that the solution of Equation (2) is a travelling wave.

**Case 2: Different motility rates, equal proliferation rates, no agent death.** If $P_m^i \neq P_m^g$ the governing PDE contains a nonlinear diffusivity term. Since the agent birth rate is independent of agent type and agents do not die, we consider the same source term as for Case 1. Again, there are no competitive or co-operative mechanisms associated with birth/death but it could be either advantageous ($P_m^i > P_m^g$) or disadvantageous ($P_m^i < P_m^g$) for an individual to be isolated from the bulk population. In this parameter regime, Equation (1) simplifies to

$$\frac{\partial C}{\partial t} = \frac{\partial}{\partial x}\left(F(C)\frac{\partial C}{\partial x}\right) + \lambda C(1 - C), \tag{6}$$

where $\lambda = \lambda_i = \lambda_g$ and $F(C) = D_i(1 - 4C + 3C^2) + D_g(4C - 3C^2)$.

bioRxiv preprint doi: https://doi.org/10.1101/077743; this version posted September 27, 2016. The copyright holder for this preprint (which was not certified by peer review) is the author/funder. All rights reserved. No reuse allowed without permission.



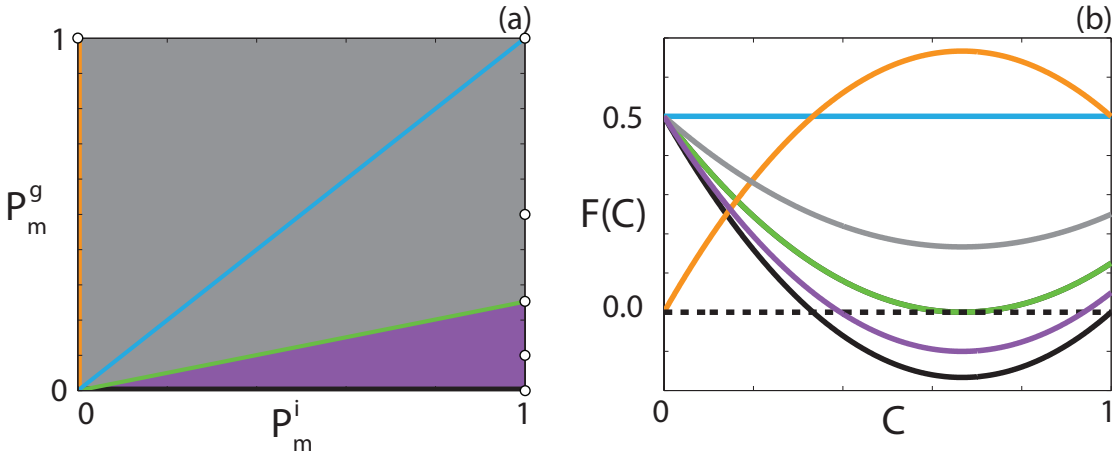


FIGURE 3. **Classification of** $F(C)$. (a) Type of $F(C)$ function for $0 \leq C \leq 1$ for the parameter space $P_m^i \in [0,1]$ and $P_m^g \in [0,1]$. The grey region represents parameter pairs that result in only positive $F(C)$, and the purple region represents parameter pairs that result in negative $F(C)$ for an interval of $C$. The orange line represents parameter pairs that result in $F(0) = 0$, the green line represents parameter pairs that result in $F(2/3) = 0$, the cyan line represents parameter pairs that result in constant $F(C)$, and the black line represents parameter pairs that result in negative $F(C)$ for an interval of $C$ with $F(1) = 0$. (b) Example $F(C)$ for each region in (a). Positive $F(C)$ (grey), corresponding to $P_m^i = 1$ and $P_m^g = 0.5$. Negative $F(C)$ for an interval of $C$ (purple), corresponding to $P_m^i = 1$ and $P_m^g = 0.1$. Negative $F(C)$ for an interval of $C$ with $F(1) = 0$ (black), corresponding to $P_m^i = 1$ and $P_m^g = 0.1$. $F(0) = 0$ (orange), corresponding to $P_m^i = 0$ and $P_m^g = 1$. $F(2/3) = 0$ (green), corresponding to $P_m^i = 1$ and $P_m^g = 0.25$. Constant $F(C)$ (cyan), corresponding to $P_m^i = 1$ and $P_m^g = 1$. The white circles in (a) denote the parameter pairs used to generate the curves in (b).

$F(C)$ has different properties depending on the choice of $P_m^i$ and $P_m^g$. To illustrate this, we present the $(P_m^i, P_m^g)$ parameter space in Figure 3(a), and highlight regions of different behaviour of $F(C)$. If $P_m^i > 4P_m^g$, there will be an interval, $1/3 \leq \alpha < C < \beta \leq 1$, centred around $C = 2/3$, where $F(C) < 0$. Specifically, this interval is given by

$$\alpha = \frac{2}{3} - \frac{\sqrt{(P_m^i)^2 - 5P_m^i P_m^g + 4(P_m^g)^2}}{3(P_m^i - P_m^g)} < C < \beta = \frac{2}{3} + \frac{\sqrt{(P_m^i)^2 - 5P_m^i P_m^g + 4(P_m^g)^2}}{3(P_m^i - P_m^g)}. \quad (7)$$

All parameter pairs that result in $F(C) < 0$, which we refer to as *positive-negative-positive*, correspond to the purple region in Figure 3(a), and an example $F(C)$ curve is given in Figure 3(b). Parameter pairs that result in $F(C) < 0$ with $F(1) = 0$ correspond to the black line in Figure 3(a), and an example $F(C)$ curve is given in Figure 3(b). We refer to this type of nonlinear diffusivity function as *capacity-degenerate positive-negative*. It is relevant for us to remark that

bioRxiv preprint doi: https://doi.org/10.1101/077743; this version posted September 27, 2016. The copyright holder for this preprint (which was not certified by peer review) is the author/funder. All rights reserved. No reuse allowed without permission.



nonlinear diffusivity functions with negative regions can lead to shocks in the solution of nonlinear diffusion equations without any source term [50, 51]. Therefore, it is instructive to consider whether shock-fronted travelling waves exist with Fisher-Kolmogorov kinetics.

For specific parameter regimes, $F(C)$ is degenerate at $C = 0$, that is, $F(0) = R(0) = 0$. This type of nonlinear diffusivity function, which we refer to as *extinction-degenerate non-negative*, leads to sharp-fronted travelling waves, provided that $F(C) \geq 0$ for $0 \leq C \leq 1$ [40, 46, 47]. For Equation (6), this corresponds to $P_m^i = 0$. The parameter pairs that satisfy this condition correspond to the orange line in Figure 3(a), and a typical $F(C)$ curve is given in Figure 3(b). The special case $P_m^i = P_m^g$ leads to a constant diffusivity, and parameter pairs that satisfy lie along the cyan line in Figure 3(a). A typical $F(C)$ curve for this case is presented in Figure 3(b). For all other parameter pairs $F(C) > 0$, which we refer to as *strictly positive*, and these parameter pairs correspond to the grey region in Figure 3(a), for which an example $F(C)$ curve is shown in Figure 3(b).

We look for a right moving travelling wave solution of Equation (6) in terms of the co-ordinate $z = x - vt$. Transforming Equation (6) into travelling wave co-ordinates, we obtain

$$v\frac{\mathrm{d}C}{\mathrm{d}z} + F(C)\frac{\mathrm{d}^2C}{\mathrm{d}z^2} + (D_i - D_g)(6C - 4)\left(\frac{\mathrm{d}C}{\mathrm{d}z}\right)^2 + \lambda C(1 - C) = 0, \quad -\infty < z < \infty. \tag{8}$$

Making the substitution $U = \mathrm{d}C/\mathrm{d}z$ gives

$$\frac{\mathrm{d}C}{\mathrm{d}z} = U, \tag{9}$$

$$\frac{\mathrm{d}U}{\mathrm{d}z} = \frac{-vU - (D_i - D_g)(6C - 4)U^2 - \lambda C(1 - C)}{F(C)}. \tag{10}$$

We now consider the properties of the travelling wave solutions for several sub-cases within Case 2. Unlike the Fisher-Kolmogorov equation, the minimum wave speed is unknown and hence all phase planes presented in this section are generated with $v$ obtained from the numerical solution of Equation (6) at sufficiently late time.

*Sub-case 2.1: Strictly positive nonlinear diffusivity function.* If $F(C) > 0$ for $0 \leq C \leq 1$, Equations (9)-(10) are not singular for $0 \leq C \leq 1$. Hence the linear analysis performed for Case 1 is valid in terms of the position and stability of the equilibrium points. The exception is the minimum wave speed condition for the equilibrium point at $(0, 0)$ to be a stable node, which

bioRxiv preprint doi: https://doi.org/10.1101/077743; this version posted September 27, 2016. The copyright holder for this preprint (which was not certified by peer review) is the author/funder. All rights reserved. No reuse allowed without permission.



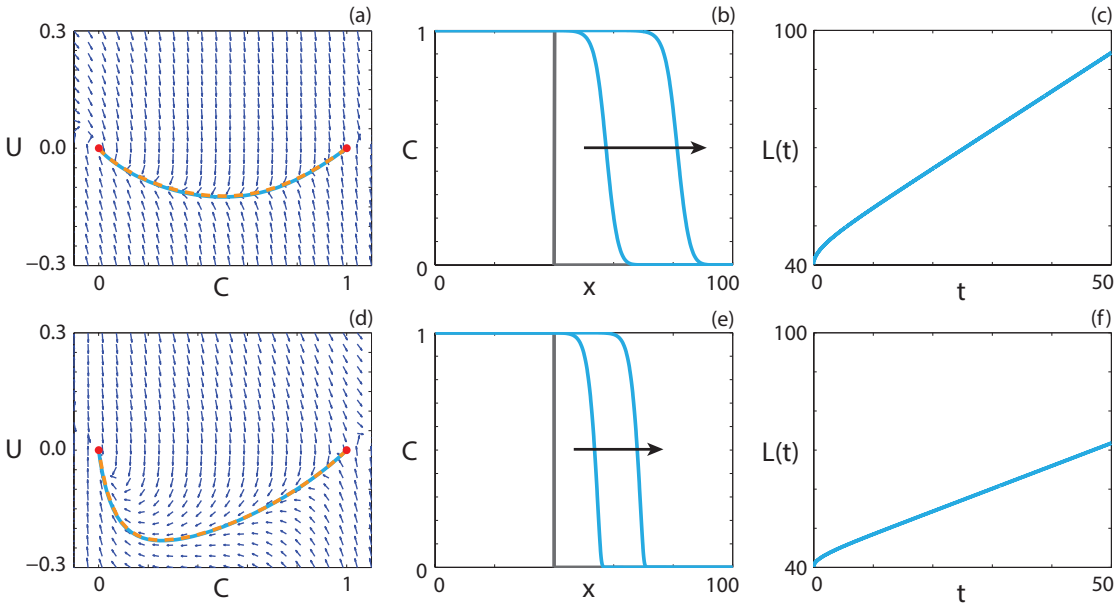


FIGURE 4. **Travelling wave behaviour for Equation** (6) **with strictly positive** $F(C)$ **(Case 2.1)**. (a), (d) Phase plane for the system (9)-(10). Red circles denote equilibrium points. The numerical solutions of Equation (6) (cyan, solid) and Equation (8) (orange, dashed), in $(C, U)$ co-ordinates, are superimposed. (b), (e) Numerical solution of Equation (6) at $t = 25$ and $t = 50$ (blue). The grey lines indicate the initial condition and the arrows indicate the direction of increasing time. (c), (f) The time evolution of the position of the leading edge of the travelling wave solution. All results are obtained using $P_p^i = P_p^g = 0.5$, $P_d^i = P_d^g = 0$, $\delta x = 0.1$, $\delta t = 0.01$, $\epsilon = 10^{-6}$ and (a)-(c) $P_m^i = 1.0$, $P_m^g = 0.5$, $v = 0.992$, (d)-(f) $P_m^i = 0.2$, $P_m^g = 0.8$, $v = 0.584$.

becomes $v > 2\sqrt{\lambda D_i}$, which is always positive [42–44].

Solutions of Equation (6), illustrating travelling wave behaviour for two different $F(C)$ functions are given in Figures 4(a)-(c) and Figures 4(d)-(f), respectively. In both cases the solution trajectory in the phase plane, Figure 4(a) and Figure 4(d), forms a heteroclinic orbit between $(1, 0)$ and $(0, 0)$. Interestingly, the waveform in Figure 4(e), with $P_m^g > P_m^i$, is relatively sharp near $C = 0$. If $P_m^g > P_m^i$, $F(C)$ is concave up with a minimum value of $P_m^i/2$ at $C = 0$, for $0 \leq C \leq 1$, whereas $F(C)$ has a minimum value at $C = 2/3$ for $P_m^i > P_m^g$. This suggests that $F(0)$ has considerable influence on the waveform.

bioRxiv preprint doi: https://doi.org/10.1101/077743; this version posted September 27, 2016. The copyright holder for this preprint (which was not certified by peer review) is the author/funder. All rights reserved. No reuse allowed without permission.



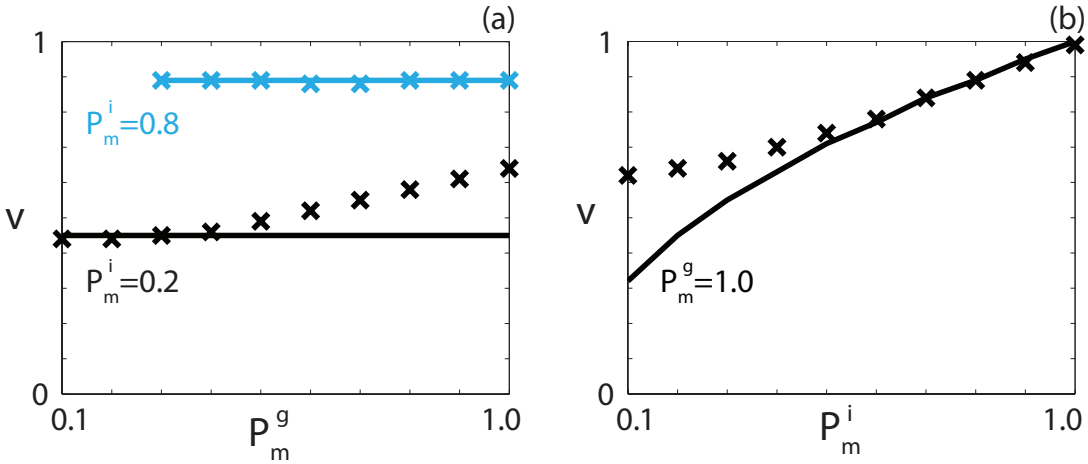


FIGURE 5. **Wave speed comparison for Case 2.1**. Comparison of the minimum wave speed condition (solid) and the observed wave speed at sufficiently late time (crosses) for (a) constant $P_m^g$ and a suite of $P_m^i$ values, and (b) constant $P_m^i$ and a suite of $P_m^g$ values. All results are obtained using $P_p^i = P_p^g = 0.5$, $P_d^i = P_d^g = 0$, $\delta x = 0.1$, $\delta t = 0.01$, $\epsilon = 10^{-6}$ and the Heaviside initial condition.

The observed wave speed in Figure 4(a), $v = 0.992$, is close to the predicted minimum wave speed $v^* = 2\sqrt{\lambda D_i} = 1$, whereas the observed wave speed in Figure 4(b), $v = 0.584$, is greater than the predicted minimum wave speed $v^* = 0.447$. To determine whether $v^*$ provides an accurate prediction of the observed wave speed, we calculate the long time numerical solution of Equation (6) and measure $v$ for a suite of $P_m^i$ and $P_m^g$ values. Predicted minimum wave speeds and observed wave speeds are compared in Figure 5. In Figure 5(a), the predicted wave speed is accurate for all $P_m^g$ values with $P_m^i = 0.8$. Interestingly, with $P_m^i = 0.2$, the predicted wave speed is only accurate for $P_m^g \leq 0.4$. Setting $P_m^g = 1$ and varying $P_m^i$ we observe, in Figure 5(b), that the prediction is accurate for $P_m^i \geq 0.5$. Hence, it appears that for $P_m^i \geq 2P_m^g$ the minimum wave speed condition is accurate. For $P_m^i < 2P_m^g$ the grouped agents may have more successful movement events than the individual agents. Therefore, the dominant contribution to the invasion of the population may be attributed to the grouped agents, which could explain why the minimum wave speed, which depends on $P_m^i$, does not provide a good estimate of the observed wave speed in these parameter regimes.

*Sub-case 2.2: Extinction-degenerate non-negative nonlinear diffusivity function.* The case where $F(0) = R(0) = 0$, and $F(C) > 0$ for $0 < C \leq 1$, occurs when $P_m^i = 0$. Under these conditions

bioRxiv preprint doi: https://doi.org/10.1101/077743; this version posted September 27, 2016. The copyright holder for this preprint (which was not certified by peer review) is the author/funder. All rights reserved. No reuse allowed without permission.



Equations (9)-(10) simplify to

$$\frac{\mathrm{d}C}{\mathrm{d}z} = U, \tag{11}$$

$$\frac{\mathrm{d}U}{\mathrm{d}z} = \frac{1}{D_g(4C-3C^2)}\Big( - vU + D_g(6C-4)U^2 - \lambda C(1-C)\Big), \quad -\infty < z < \infty. \tag{12}$$

Note that Equation (12) is singular at $C = 0$ and, furthermore, that $R(0) = 0$. Hence we apply a stretching transformation

$$\zeta = \int_0^z \frac{1}{D_g(4C(s)-3C(s)^2)}\,\mathrm{d}s, \tag{13}$$

to remove the singularity, which gives

$$\frac{\mathrm{d}C}{\mathrm{d}\zeta} = D_g U(4C-3C^2), \tag{14}$$

$$\frac{\mathrm{d}U}{\mathrm{d}\zeta} = -vU + D_g(6C-4)U^2 - \lambda C(1-C),\ \zeta \geq 0. \tag{15}$$

Equations (14)-(15) have equilibrium points at $(C, U) = (1, 0)$, $(C, U) = (0, 0)$ and $(C, U) = (0, -v/4D_g)$. The additional equilibrium point in the transformed system corresponds to a solution trajectory approaching $C = 0$ with a non-zero slope. Performing linear analysis to determine the eigenvalues of the Jacobian at the steady states, we find that the characteristic equation at $(0, 0)$ has solutions $\xi = 0$ and $\xi = v$, implying that $(0, 0)$ is an improper node. Sánchez-Garduño and Maini [40] investigate the stability of this equilibrium point and find that the equilibrium point is a saddle node. The characteristic equation at $(1, 0)$ has solutions $\xi = (-v \pm \sqrt{v^2 + 4\lambda D_g})/2$, implying that $(1, 0)$ is a saddle point. Finally the characteristic equation of the equilibrium point at $(0, -v/4D_g)$ has eigenvalues $\xi = \pm v$, implying that $(0, -v/4D_g)$ is a saddle point. A critical value $v^*$ exists such that $v < v^*$ results in no travelling wave solution, $v = v^*$ results in a sharp-fronted travelling wave and $v > v^*$ results in a classic (smooth) travelling wave [40].

Numerical solutions illustrating travelling wave behaviour for Equation (6) with $P_m^i = 0$ are given in Figure 6. In the phase plane for both cases, Figure 6(a) and Figure 6(d), the solution trajectory tends to the origin with $\mathrm{d}U/\mathrm{d}C$ large and negative. The corresponding numerical solutions of Equation (6), presented in Figure 6(b) and Figure 6(e), approach a travelling wave solution with a sharp front near $C = 0$. This result is expected as the Heaviside initial condition results in

bioRxiv preprint doi: https://doi.org/10.1101/077743; this version posted September 27, 2016. The copyright holder for this preprint (which was not certified by peer review) is the author/funder. All rights reserved. No reuse allowed without permission.



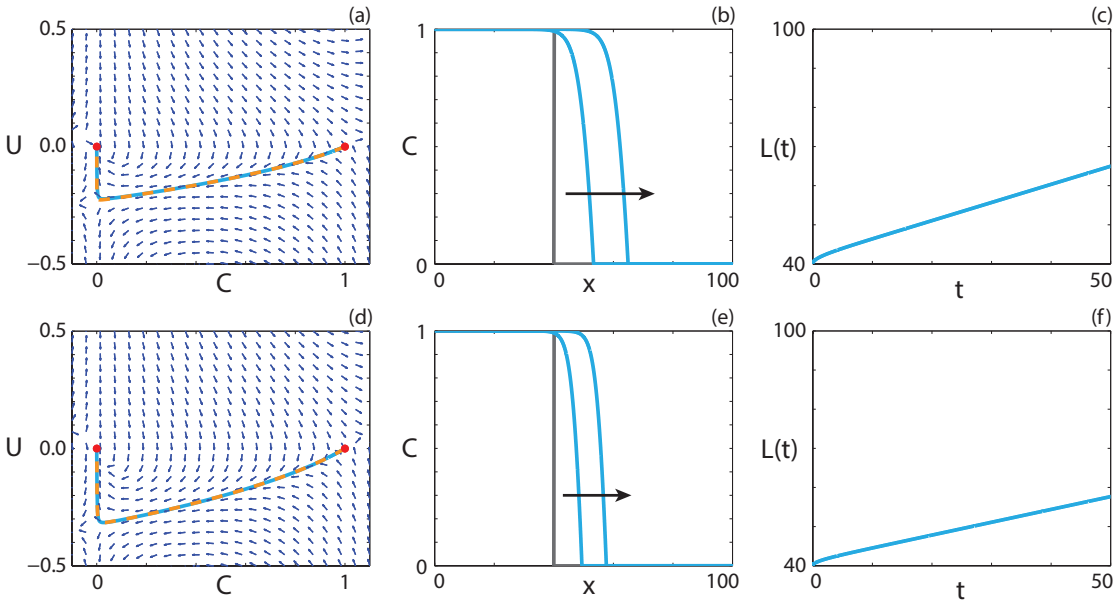


FIGURE 6. **Travelling wave behaviour for Equation** (6) **with extinction-degenerate non-negative** $F(C)$ **(Case 2.2)**. (a), (d) Phase plane for the system (11)-(12). Red circles denote equilibrium points. The numerical solutions of Equations (6) (cyan, solid) and (8) (orange, dashed), in $(C, U)$ co-ordinates, are superimposed. (b), (e) Numerical solution of Equation (6) at $t = 25$ and $t = 50$. The grey lines indicate the initial condition and the arrows indicate the direction of increasing time. (c), (f) The time evolution of the position of the leading edge of the travelling wave solution. All results are obtained using $P_m^i = 0$, $P_p^i = P_p^g = 0.3$, $P_d^g = P_d^i = 0$, $\delta x = 0.01$, $\delta t = 0.01$, $\epsilon = 10^{-6}$ and (a)-(c) $P_m^g = 1.0$, $v = 0.463$, (d)-(f) $P_m^g = 0.5$, $v = 0.328$.

the minimum wave speed that, for a degenerate diffusivity function, results in a sharp-fronted wave [46].

*Sub-case 2.3: Positive-negative-positive nonlinear diffusivity function.* In order for $F(C)$ to change sign twice, that is, $F(C) < 0$ for $1/3 \leq \alpha < C < \beta \leq 1$ and $F(C) \geq 0$ otherwise for $0 \leq C \leq 1$, the parameters must lie within the purple region in Figure 3(a). In this situation, Equations (9)-(10) are undefined at $C = \alpha$ and $C = \beta$, and these singularities cannot be removed using a stretching transformation since $R(\alpha) \neq 0$ and $R(\beta) \neq 0$. However, it is possible

bioRxiv preprint doi: https://doi.org/10.1101/077743; this version posted September 27, 2016. The copyright holder for this preprint (which was not certified by peer review) is the author/funder. All rights reserved. No reuse allowed without permission.



for $\mathrm{d}U/\mathrm{d}z$ to be finite at $C = \alpha$ and $C = \beta$ if $U_\alpha$ and $U_\beta$ exist such that

$$\lim_{C\to\alpha}\left[\frac{-vU_\alpha - (D_i - D_g)(6C-4)U_\alpha^2 - \lambda C(1-C)}{D_i(1-4C+3C^2) + D_g(4C-3C^2)}\right], \tag{16}$$

$$\lim_{C\to\beta}\left[\frac{-vU_\beta - (D_i - D_g)(6C-4)U_\beta^2 - \lambda C(1-C)}{D_i(1-4C+3C^2) + D_g(4C-3C^2)}\right], \tag{17}$$

are both finite. This requires the numerator in the expressions (16)-(17) vanish at $C = \alpha$ and $C = \beta$, respectively. As such, $U_\alpha$ and $U_\beta$ are obtained by solving the system

$$0 = -vU_\alpha - (D_i - D_g)(6\alpha - 4)U_\alpha^2 - \lambda\alpha(1-\alpha), \tag{18}$$

$$0 = -vU_\beta - (D_i - D_g)(6\beta - 4)U_\beta^2 - \lambda\beta(1-\beta), \tag{19}$$

resulting in $U_\alpha = -(v \pm \sqrt{v^2 - 4F'(\alpha)R(\alpha)})/2F'(\alpha)$ and $U_\beta = -(v \pm \sqrt{v^2 - 4F'(\beta)R(\beta)})/2F'(\beta)$. We note that as $R(C) \geq 0$ for $0 \leq C \leq 1$, and that $F'(\alpha) \leq 0$ for all possible $\alpha$ values, $U_\alpha$ will be real-valued. Subsequently, we have a wave speed condition that $v \geq 2\sqrt{F'(\beta)R(\beta)}$, as $F'(\beta) \geq 0$ for all possible $\beta$ values. Ferracuti *et al.* [36] prove that the minimum wave speed, $v^*$, is greater than a threshold value, which in turn is greater than $\max\{R'(0)F(0), F'(\beta)R(\beta)\}$. Therefore, $U_\beta$ will also always be real-valued.

Applying L'Hopital's Rule to Equation (10), we obtain

$$\lim_{C\to\alpha}\left.\frac{\mathrm{d}U}{\mathrm{d}z}\right|_{U=U_\alpha} = \lim_{C\to\alpha}\left[\frac{6(D_i - D_g)U_\alpha^2 + \lambda(1-2C)}{(D_g - D_i)(6C-4)}\right], \tag{20}$$

$$\lim_{C\to\beta}\left.\frac{\mathrm{d}U}{\mathrm{d}z}\right|_{U=U_\beta} = \lim_{C\to\beta}\left[\frac{6(D_i - D_g)U_\beta^2 + \lambda(1-2C)}{(D_g - D_i)(6C-4)}\right], \tag{21}$$

which are finite provided that $\alpha \neq 2/3$ and $\beta \neq 2/3$. For the system of Equations (9)-(10), we have two straight lines in the phase plane where $\mathrm{d}U/\mathrm{d}z$ is infinite, at $C = \alpha$ and $C = \beta$. These kind of lines have previously been called *walls of singularities* for hyperbolic models related to chemotactic and haptotactic invasion [52]. For a smooth solution trajectory to exist between two equilibrium points on opposite sides of the wall of singularities, we require that the trajectory passes through the wall of singularities. This implies that the solution trajectory must pass through the wall of singularities at the special points, $(\alpha, U_\alpha)$ and $(\beta, U_\beta)$, known as holes in the wall [52, 53]. Otherwise, a smooth heteroclinic orbit between $(1, 0)$ and $(0, 0)$ cannot exist, as $\lim_{C\to\alpha}|U| \to \infty$ and $\lim_{C\to\beta}|U| \to \infty$. As $U_\alpha$ and $U_\beta$ are real valued and the limits in

bioRxiv preprint doi: https://doi.org/10.1101/077743; this version posted September 27, 2016. The copyright holder for this preprint (which was not certified by peer review) is the author/funder. All rights reserved. No reuse allowed without permission.



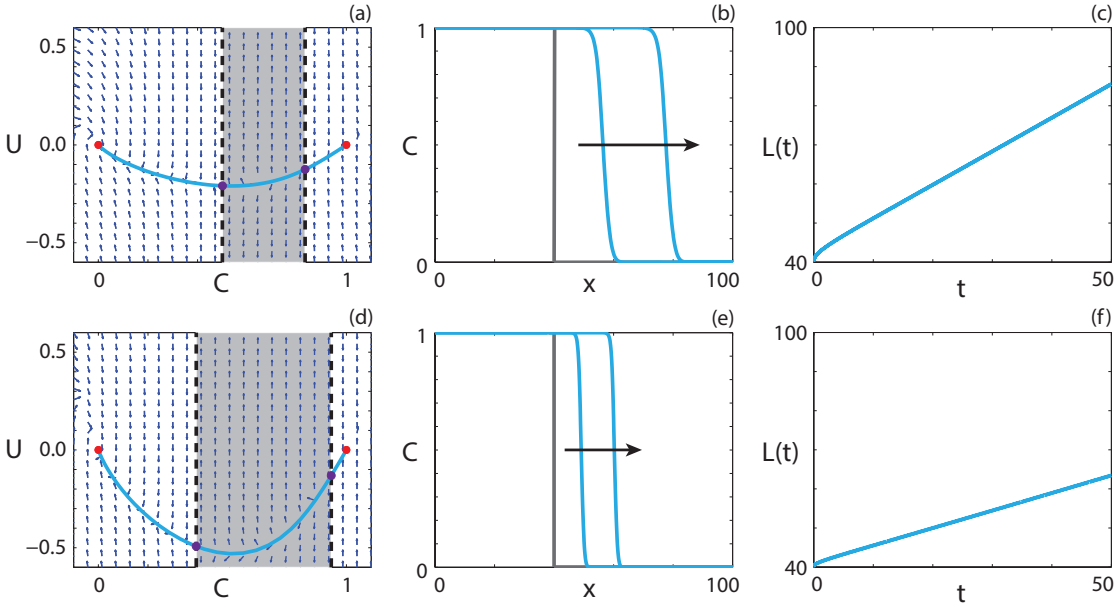


FIGURE 7. **Travelling wave behaviour for Equation** (6) **with positive-negative-positive** $F(C)$ **(Case 2.3)**. (a), (d) Phase plane for the system (9)-(10) with the numerical solution of Equation (6), in $(C, U)$ co-ordinates, superimposed. The grey region corresponds to values of $C$ where $F(C) < 0$. The dashed black lines denote a wall of singularities. Red circles correspond to equilibrium points and purple circles correspond to holes in the wall. (b), (e) Numerical solution of Equation (6) at $t = 100$ and $t = 200$. The grey lines indicate the initial condition and the arrows indicate the direction of increasing time. (c), (f) The time evolution of the position of the leading edge of the travelling wave solution, $L(t)$. All results are obtained using $P_d^i = P_d^g = 0$, $\delta x = 0.01$, $\delta t = 0.01$, $\epsilon = 10^{-6}$ and (a)-(c) $P_m^i = 0.5$, $P_m^g = 0.1$, $P_p^i = P_p^g = 0.75$, $v = 0.864$, (d)-(f) $P_m^i = 0.1$, $P_m^g = 0.01$, $P_p^i = P_p^g = 1.0$, $v = 0.448$.

Equations (20)-(21) are finite, the holes in the wall always exist for Fisher kinetics.

Ferracuti *et al.* [36] prove that travelling wave solutions exist for reaction-diffusion equations with positive-negative-positive $F(C)$ and Fisher kinetics, however travelling wave profiles arising from the PDE are not presented. An upper bound on the minimum wave speed is stated as [36]

$$v^* = \max\{v_1, v_2, v_3\}, \tag{22}$$

bioRxiv preprint doi: https://doi.org/10.1101/077743; this version posted September 27, 2016. The copyright holder for this preprint (which was not certified by peer review) is the author/funder. All rights reserved. No reuse allowed without permission.



where

$$F'(0)R(0) + F(0)R'(0) \leq \frac{v_1^2}{4} \leq \sup_{C\in(0,\alpha]} \left[\frac{F(C)R(C)}{C}\right], \tag{23}$$

$$F'(\beta)R(\beta) + F(\beta)R'(\beta) \leq \frac{v_2^2}{4} \leq \sup_{C\in[\alpha,\beta)} \left[\frac{F(C)R(C)}{C-\beta}\right], \tag{24}$$

$$F'(\beta)R(\beta) + F(\beta)R'(\beta) \leq \frac{v_3^2}{4} \leq \sup_{C\in(\beta,1]} \left[\frac{F(C)R(C)}{C-\beta}\right], \tag{25}$$

where the prime denotes ordinary differentiation with respect to $C$. Numerical solutions of Equation (6) with $P_m^i > 4P_m^g$ are presented in Figure 7. We superimpose the numerical solution of Equation (6) in $(C, U)$ co-ordinates on the phase plane for the system (9)-(10) in Figures 7(a) and 7(d). The numerical solution forms a heteroclinic orbit between $(1, 0)$ and $(0, 0)$ in both cases, and passes through the holes in the wall of singularities, denoted using purple circles. Continuum models with negative diffusivity and no source terms have been relatively well studied, and exhibit shock behaviour across the region of negative diffusion [50,51]. Interestingly, our solution does not include a shock and is instead smooth through the region of negative diffusion.

Numerical solutions of Equation (6) are presented in Figures 7(b) and 7(e), which appear to take the form of travelling waves. The observed wave speeds, $v = 0.864$ and $v = 0.456$, in Figure 7(c) and Figure 7(f), respectively, are well approximated by the upper bound on the minimum wave speed presented by Ferracuti *et al.* [36]. The bound provides values for the minimum wave speed of $v^* = 0.866$ and $v^* = 0.447$, respectively. We might expect that the observed wave speeds correspond to the minimum wave speeds since the initial conditions for the numerical solutions are given by a Heaviside initial condition.

The observed wave speed, obtained from the long time numerical solutions of Equation (6), and the upper bound on the minimum wave speed, given by Equation (22), are shown in Figure 8 for a suite of $P_p$ values and two positive-negative-positive $F(C)$ functions. In all cases the bound provides an accurate prediction of the observed wave speed.

*Sub-case 2.4: Capacity-degenerate positive-negative nonlinear diffusivity function.* For the special case where $P_m^g = 0$, $F(1) = 0$. As $F(C)$ is degenerate at $C = 1$, it is intuitive to expect there could be sharp-fronted travelling wave solutions, with the sharp front near $C = 1$, similar to the results in Figure 6. However, unlike for the parameter regimes in Figure 6, we have an interval

bioRxiv preprint doi: https://doi.org/10.1101/077743; this version posted September 27, 2016. The copyright holder for this preprint (which was not certified by peer review) is the author/funder. All rights reserved. No reuse allowed without permission.



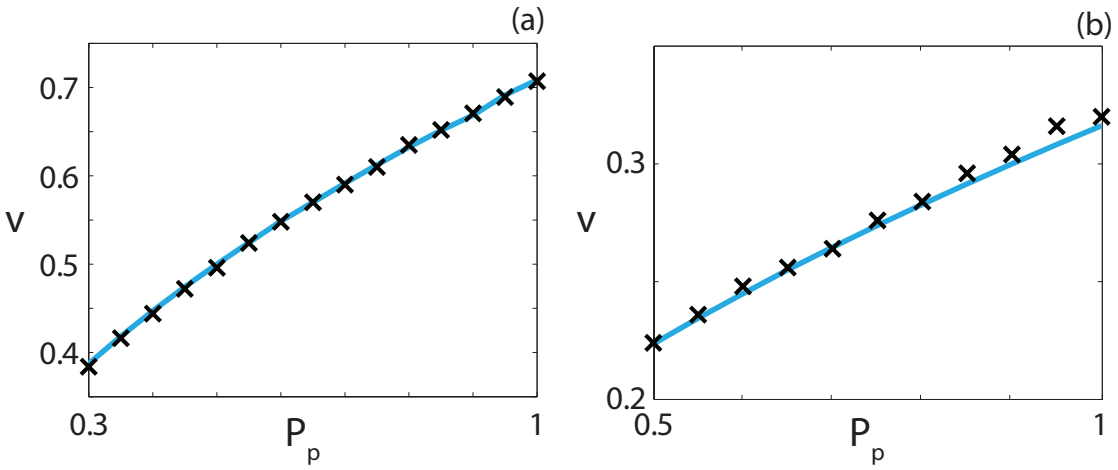


FIGURE 8. **Wave speed comparison for Case 2.3**. Comparison of the observed wave speed and the upper bound of the minimum wave speed obtained from the relationship in Equation (22) for a suite of $P_p$ values. All results are obtained using $P_d^i = P_d^g = 0$, $\delta x = 0.01$, $\delta t = 0.01$, $\epsilon = 10^{-6}$, and (a) $P_m^i = 0.25$, $P_m^g = 0.05$, (b) $P_m^i = 0.05$, $P_m^g = 0.005$, and the Heaviside initial condition. In all cases Equation (23) provided the estimate of the minimum wave speed. Crosses correspond to the observed wave speed and the solid line corresponds to the upper bound of the wave speed.

$1/3 < C < 1$ where $F(C) < 0$. To determine whether this negative diffusivity influences the presence of sharp fronts, we follow the approach of Maini *et al.* [38], who show that the existence of travelling waves for reaction-diffusion equations with capacity-degenerate positive-negative $F(C)$ can be determined by considering the existence of travelling waves for

$$\frac{\partial C}{\partial \hat{t}} = \frac{\partial^2 C}{\partial x^2} + F(C)R(C), \ \hat{t} \geq 0. \tag{26}$$

The restriction on $\hat{t}$ implies that $F(C) > 0$. As $F(C) < 0$ for $1/3 < C < 1$, Equation (26) is only equivalent to Equation (6) for $0 \leq C \leq 1/3$. For $1/3 \leq C \leq 1$, Equation (6) is equivalent to

$$\frac{\partial C}{\partial \hat{t}} = \frac{\partial^2 C}{\partial x^2} + \hat{F}(C)\hat{R}(C), \ \hat{t} \geq 0, \tag{27}$$

where $\hat{F}(C) = -F(1-C)$ and $\hat{R}(C) = R(1-C)$ [38]. Equations (26)-(27) have minimum travelling wave speeds $v_0^*$ and $v_1^*$, respectively. Maini *et al.* [38] prove that sharp fronts in the travelling wave near $C = 1$ only exist if $F(1) = 0$ and $v_1^* < v_0^*$. The first condition is obviously satisfied, while the second can be determined through linear analysis of Equations (26)-(27) in travelling wave co-ordinates. Both equations have minimum wave speed conditions, $v_0^* = v_1^* = 2\sqrt{\lambda D_i}$, to obtain physically-relevant heteroclinic orbits, and hence travelling wave solutions with a sharp

bioRxiv preprint doi: https://doi.org/10.1101/077743; this version posted September 27, 2016. The copyright holder for this preprint (which was not certified by peer review) is the author/funder. All rights reserved. No reuse allowed without permission.



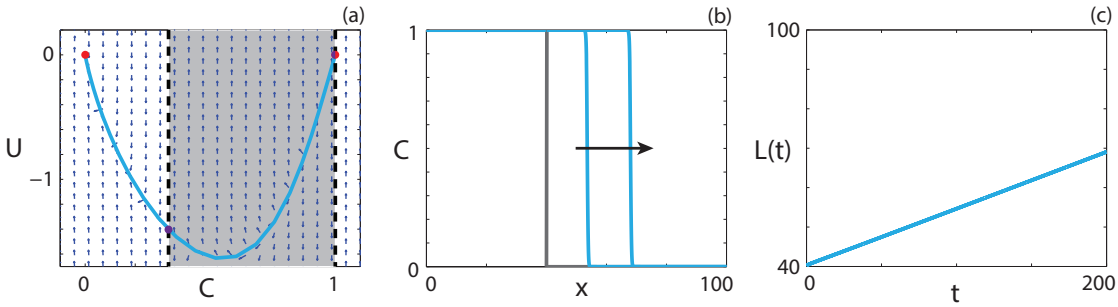


FIGURE 9. **Travelling wave behaviour for Equation** (6) **with capacity-degenerate positive-negative** $F(C)$ **(Case 2.4)**. (a) Phase plane for the system (9)-(10) with the numerical solution of Equation (6), in $(C, U)$ co-ordinates, superimposed. The grey region corresponds to values of $C$ where $F(C) < 0$. The dashed black lines denote a wall of singularities. Red circles correspond to equilibrium points and purple circles correspond to holes in the wall. (b) Numerical solution of Equation (6) at $t = 100$ and $t = 200$. The grey lines indicate the initial condition and the arrow indicates the direction of increasing time. (c) The time evolution of the position of the leading edge of the travelling wave solution, $L(t)$. All results are obtained using $P_m^i = 0.01$, $P_m^g = 0$, $P_p^i = P_p^g = 1.0$, $P_d^i = P_d^g = 0$, $\delta x = 0.01$, $\delta t = 0.01$, $\epsilon = 10^{-6}$, $v = 0.1433$.

region near $C = 1$ do not exist.

Travelling wave behaviour for a parameter regime with $F(1) = 0$ is shown in Figure 9. The equilibrium point at $(1, 0)$ is also a hole in the wall. The solution trajectory forms a heteroclinic orbit between $(1, 0)$ and $(0, 0)$, and moves through the region of $C$ where $F(C) < 0$. Although $F(1) = 0$, we do not observe a solution trajectory corresponding to a sharp front, as we observed in Figure 6, where $F(0) = 0$. This result is consistent with the analysis of Maini *et al.* [38]. The numerical solution of Equation (9), presented in Figure 9(b), has a relatively steep front but is not sharp near $C = 1$. As $L(t)$, presented in Figure 9(c), becomes linear as $t$ increases and the waveform in Figure 9(b) are consistent, the numerical solution of Equation (6) with $F(1) = 0$ appears to form a classic travelling wave.

**Case 3: Equal motility rates, equal proliferation rates, equal death rates.** For $P_d^i = P_d^g > 0$, with $P_m^i = P_m^g$ and $P_p^i = P_p^g$, there are no competitive or co-operative mechanisms. In this case, Equation (1) becomes

$$\frac{\partial C}{\partial t} = D\frac{\partial^2 C}{\partial x^2} + \lambda C(1 - C) - KC, \tag{28}$$

bioRxiv preprint doi: https://doi.org/10.1101/077743; this version posted September 27, 2016. The copyright holder for this preprint (which was not certified by peer review) is the author/funder. All rights reserved. No reuse allowed without permission.



where $D = D_i = D_g$, $\lambda = \lambda_i = \lambda_g$ and $K = K_i = K_g$. The corresponding ODE in travelling wave co-ordinates is

$$D\frac{\mathrm{d}^2C}{\mathrm{d}z^2} + v\frac{\mathrm{d}C}{\mathrm{d}z} + \lambda C(1-C) - KC = 0, \ -\infty < z < \infty, \tag{29}$$

and, with $U = \mathrm{d}C/\mathrm{d}z$, we obtain

$$\frac{\mathrm{d}C}{\mathrm{d}z} = U, \tag{30}$$

$$\frac{\mathrm{d}U}{\mathrm{d}z} = -\frac{v}{D}U - \frac{\lambda}{D}C(1-C) + \frac{K}{D}C. \tag{31}$$

The source term in Equation (28) is non-positive for all relevant $C$ values if $K > \lambda$, and negative for $C > (\lambda - K)/\lambda$ otherwise. Hence the population will never reach the original carrying capacity of unity. The new carrying capacity can be determined by considering the zeros of the source term, which occur at $C = 0$ and $C = (\lambda - K)/\lambda$. Introducing a new variable, $\overline{C} = \lambda C/(\lambda - K)$, and rewriting Equation (28) in terms of $\overline{C}$ we obtain

$$\frac{\partial \overline{C}}{\partial t} = D\frac{\partial^2 \overline{C}}{\partial x^2} + (\lambda - K)\overline{C}(1-\overline{C}). \tag{32}$$

Equation (32) is the Fisher-Kolmogorov equation in terms of the new variable, $\overline{C}$, with an intrinsic growth rate $(\lambda - K)$. As such, the analysis performed for Case 1 is applicable here and we obtain information about the stability of the equilibrium points, as well as the minimum wave speed required for physically meaningful travelling wave solutions. If $\lambda > K$, the minimum wave speed is $v^* = 2\sqrt{(\lambda - K)D}$. If $K > \lambda$, there is only one physically relevant equilibrium point, $C = 0$, and hence the population will tend to extinction and travelling wave solutions do not exist.

Travelling wave behaviour for two parameter regimes with $\lambda > K$ are illustrated in Figure 10. The phase plane for $K = 0.1$, presented in Figure 10(a), displays qualitatively similar behaviour to the phase plane for $K = 0.2$, presented in Figure 10(d). Unsurprisingly, the unstable equilibrium point moves closer to zero as $K$ approaches $\lambda$. The numerical solutions of Equation (28), presented in Figures 10(b) and 10(e), have significantly different densities behind the wave fronts. However, both travelling wave fronts represent heteroclinic orbits between $(C, U) = ((\lambda - K)/\lambda, 0)$ and $(C, U) = (0, 0)$. Interestingly, the two travelling wave fronts have approximately the same support, even though the waveform is significantly shallower for the case with $K = 0.2$. Results in Figures 10(c) and (f) show that both solutions approach travelling waves as $t$ increases, and that increasing the death rate reduces the wave speed.

bioRxiv preprint doi: https://doi.org/10.1101/077743; this version posted September 27, 2016. The copyright holder for this preprint (which was not certified by peer review) is the author/funder. All rights reserved. No reuse allowed without permission.



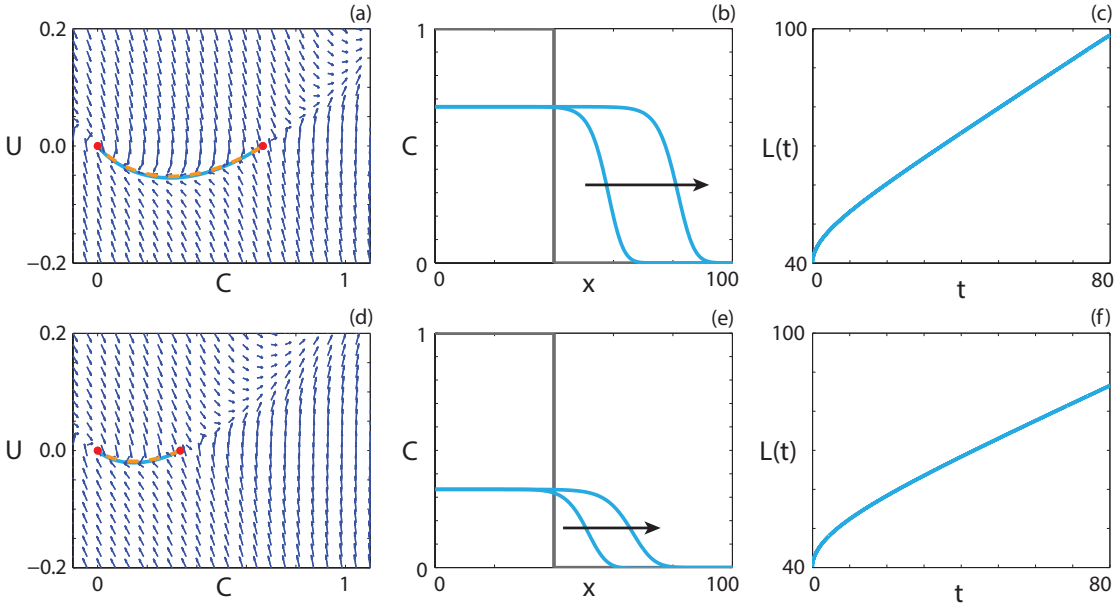


FIGURE 10. **Travelling wave behaviour for the scaled Fisher-Kolmogorov model (Case 3)**. (a), (d) Phase plane for the system (30)-(31). Red circles denote equilibrium points. The numerical solutions of Equations (28) (cyan, solid) and (29) (orange, dashed), in $(C, U)$ co-ordinates, are superimposed. (b), (e) Numerical solution of Equation (28) at $t = 40$ and $t = 80$. The grey lines indicate the initial condition and the arrows indicate the direction of increasing time. (c), (f) The time evolution of the position of the leading edge of the travelling wave solution. All results are obtained using $P_m^i = P_m^g = 1$, $P_p^i = P_p^g = 0.3$, $\delta x = 0.1$, $\delta t = 0.01$, $\epsilon = 10^{-6}$ and (a)-(c) $P_d^g = P_d^i = 0.1$, $v = 0.615$, (d)-(f) $P_d^g = P_d^i = 0.2$, $v = 0.445$.

**Case 4: Different motility rates, equal proliferation rates, equal death rates.** For $P_p^i = P_p^g$, $P_d^i = P_d^g$ and $P_m^i \neq P_m^g$, the co-operative or competitive mechanism arises due to the difference in the rate of motility. In this case, the governing PDE is

$$\frac{\partial C}{\partial t} = \frac{\partial}{\partial x}\left(F(C)\frac{\partial C}{\partial x}\right) + \lambda C(1-C) - KC, \tag{33}$$

where $F(C) = D_i(1 - 4C + 3C^2) + D_g(4C - 3C^2)$, $\lambda = \lambda_i = \lambda_g$ and $K = K_i = K_g$. Equation (33) corresponds to

$$v\frac{\mathrm{d}C}{\mathrm{d}z} + F(C)\frac{\mathrm{d}^2C}{\mathrm{d}z^2} + (D_i - D_g)(6C-4)\left(\frac{\mathrm{d}C}{\mathrm{d}z}\right)^2 + \lambda C(1-C) - KC = 0, \ -\infty < z < \infty, \tag{34}$$

bioRxiv preprint doi: https://doi.org/10.1101/077743; this version posted September 27, 2016. The copyright holder for this preprint (which was not certified by peer review) is the author/funder. All rights reserved. No reuse allowed without permission.



in travelling wave co-ordinates, and with the substitution $U = \mathrm{d}C/\mathrm{d}z$, we obtain

$$\frac{\mathrm{d}C}{\mathrm{d}z} = U, \tag{35}$$

$$\frac{\mathrm{d}U}{\mathrm{d}z} = \frac{-vU - (D_i - D_g)(6C-4)U^2 - \lambda C(1-C) + KC}{F(C)}. \tag{36}$$

The system of Equations (35)-(36) has equilibrium points $(C, U) = (0, 0)$ and $(C, U) = (S, 0)$, where $S = (\lambda - K)/\lambda$. Increasing $K$ causes a decrease in the carrying capacity, $S$. If $K > \lambda$, the non-zero equilibrium point occurs at a negative $C$ value and hence only one physically relevant equilibrium point exists, implying that the population will become extinct. Hence we only investigate the behaviour of parameter regimes where $\lambda > K$.

We introduce the variable $\overline{C} = C/S$ such that the agent density is scaled by the carrying capacity and, subsequently, the zeros of the source term occur at $\overline{C} = 0$ and $\overline{C} = 1$. This approach allows us to repeat the analysis for Case 2 with a different $F(C)$. We transform Equation (33) in terms of $\overline{C}$ to obtain

$$\frac{\partial \overline{C}}{\partial t} = \frac{\partial}{\partial x}\left(F(S\overline{C})\frac{\partial \overline{C}}{\partial x}\right) + (\lambda - K)\overline{C}(1-\overline{C}). \tag{37}$$

If we define $\overline{U} = \mathrm{d}\overline{C}/\mathrm{d}z$, Equation (37) corresponds to the system,

$$\frac{\mathrm{d}\overline{C}}{\mathrm{d}z} = \overline{U}, \tag{38}$$

$$\frac{\mathrm{d}\overline{U}}{\mathrm{d}z} = \frac{-v\overline{U} - (D_i - D_g)S(6S\overline{C}-4)\overline{U}^2 - (\lambda - K)\overline{C}(1-\overline{C})}{F(S\overline{C})}, \quad -\infty < z < \infty. \tag{39}$$

The transformed nonlinear diffusivity function

$$F_s(\overline{C}) = F(S\overline{C}) = D_i(1 - 4S\overline{C} + 3(S\overline{C})^2) + D_g(4S\overline{C} - 3(S\overline{C})^2), \tag{40}$$

has different properties depending on $S$, $D_i$ and $D_g$. To highlight this, Figure 11 shows the $(P_m^i, P_m^g)$ parameter space for three different $S$ values and the qualitative behaviour of the corresponding $F_s(\overline{C})$ function. For $S = 1$, presented in Figure 11(a), we recover the nonlinear diffusivity function examined for Case 2, where for $P_m^i > 4P_m^g$, denoted in purple, there is an interval $\alpha < \overline{C} < \beta$, $\alpha < \beta < 1$, where $F_s(\overline{C}) < 0$. Decreasing $S$ to 0.9, presented in Figure 11(b), we observe that the purple region again occurs for $P_m^i > 4P_m^g$. However, if $P_m^g < 0.145P_m^i$, highlighted in red, $F_s(\overline{C}) < 0$ for $\omega < \overline{C} \leq 1$, and hence $F_s(\overline{C})$ has only one zero in $0 \leq \overline{C} \leq 1$. This type of nonlinear diffusivity function is not observed for Case 2 and we refer to it as *positive-negative*. Specifically, this behaviour occurs when $(16 - (6S-4)^2)P_m^g < (4 - (6S-4)^2)P_m^i$ and

bioRxiv preprint doi: https://doi.org/10.1101/077743; this version posted September 27, 2016. The copyright holder for this preprint (which was not certified by peer review) is the author/funder. All rights reserved. No reuse allowed without permission.



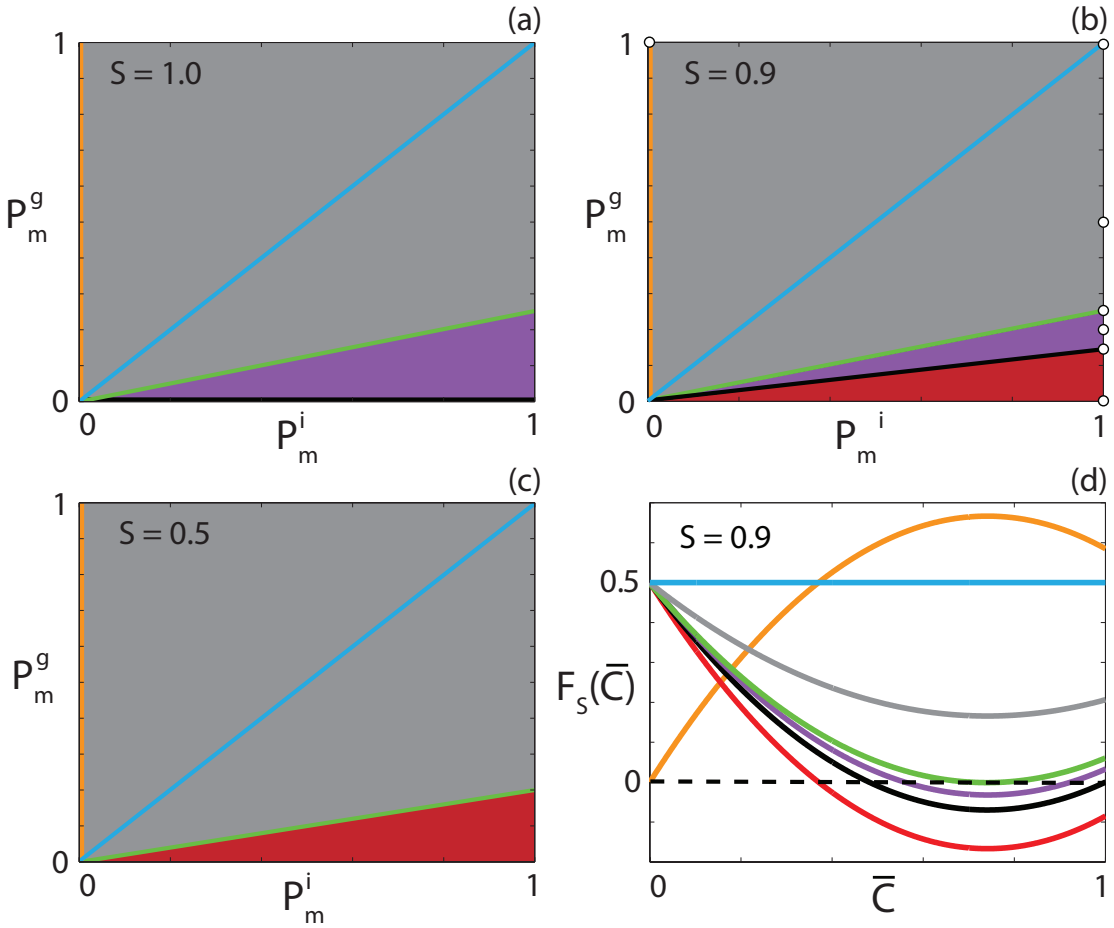


FIGURE 11. **Classification of** $F_s(\overline{C})$ for different carrying capacity densities. (a)-(c) Type of $F_s(\overline{C})$ function for $0 \leq \overline{C} \leq 1$ for the parameter space $P_m^i \in [0,1]$ and $P_m^g \in [0,1]$ with (a) $S = 1.0$, (b) $S = 0.9$ and (c) $S = 0.5$. Grey regions correspond to parameter pairs that result in strictly positive $F_s(\overline{C})$, purple regions correspond to parameter pairs that result in positive-negative-positive $F_s(\overline{C})$ and red regions correspond to parameter pairs that result in positive-negative $F_s(\overline{C})$. Cyan, orange and black lines correspond to constant, extinction-degenerate non-negative and capacity-degenerate positive-negative $F_s(\overline{C})$ curves, respectively. (d) Example $F_s(\overline{C})$ for each region in (b). The white circles in (b) denote the parameter pairs used to generate the curves in (d).

$P_m^i > 4P_m^g$. Furthermore, this implies that for $S < 2/3$ there are no $(P_m^i, P_m^g)$ values that correspond to positive-negative-positive $F_s(\overline{C})$. An example of this $(P_m^i, P_m^g)$ parameter space is shown in Figure 11(c). For $S < 1/3$, $F_s(\overline{C}) \geq 0$ for $0 \leq \overline{C} \leq 1$. Parameter pairs that correspond to extinction-degenerate non-negative $F_s(\overline{C})$ (orange) and constant $F_s(\overline{C})$ (cyan) exist for all $S$

bioRxiv preprint doi: https://doi.org/10.1101/077743; this version posted September 27, 2016. The copyright holder for this preprint (which was not certified by peer review) is the author/funder. All rights reserved. No reuse allowed without permission.



values.

*Sub-case 4.1: Strictly positive nonlinear diffusivity function.* If $F_s(\overline{C}) > 0$ for $0 \leq \overline{C} \leq 1$, linear analysis leads to a minimum wave speed $v^* = 2\sqrt{(\lambda - K)D_i}$ for the equilibrium point at $(0, 0)$ to be stable. Intuitively, the wave speed is positive provided that the rate of birth is greater than the rate of death.

Travelling wave behaviour for Equation (33) with strictly positive $F_s(\overline{C})$ and $S = 0.5$ is shown in Figures 12(a)-(c). Similar to the strictly positive $F(C)$ considered in Case 2.1, there is a heteroclinic orbit between the two equilibrium points, implying that the solution of Equation (33) forms a travelling wave. Intuitively, introducing agent death has the effect of reducing the density sufficiently far behind the wave front, and we observe that the non-zero equilibrium point now occurs at $C = S \leq 1$.

*Sub-case 4.2: Extinction-degenerate non-negative nonlinear diffusivity function.* If $F_s(0) = 0$, $F_s(\overline{C}) > 0$ for $0 < \overline{C} \leq 1$, and $R(0) = 0$, a stretching transformation is applied to remove the singularity in Equations (38)-(39), giving

$$\frac{\mathrm{d}\overline{C}}{\mathrm{d}\zeta} = D_g S(4\overline{C} - 3S\overline{C}^2)\overline{U}, \tag{41}$$

$$\frac{\mathrm{d}\overline{U}}{\mathrm{d}\zeta} = -v\overline{U} + D_g S(6S\overline{C} - 4)\overline{U}^2 - (\lambda - K)\overline{C}(1 - \overline{C}), \ \zeta \geq 0, \tag{42}$$

as $D_i = 0$. There are now three equilibrium points: $(\overline{C}, \overline{U}) = (0, 0)$; $(\overline{C}, \overline{U}) = (1, 0)$; and $(\overline{C}, \overline{U}) = (0, -v/4SD_g)$. As for Case 2.2, the saddle-saddle connection between $(1, 0)$ and $(0, -v/4SD_g)$ only occurs for a unique wave speed $v^*$, which implies that sharp-fronted solutions exist only for the minimum wave speed.

Sharp-fronted travelling wave solutions of Equation (33) with extinction-degenerate non-negative $F_s(\overline{C})$ and $S = 0.9$ are shown in Figures 12(d)-(f). Introducing agent death does not change the qualitative behaviour compared to the corresponding case with $K = 0$ (Case 2.2). Specifically, $\mathrm{d}C/\mathrm{d}z$ approaches $C = 0$ with a non-zero value and hence the wave front is sharp near $C = 0$. Again, the density behind the wave front decreases such that $C = S$, corresponding to the non-zero equilibrium point.

bioRxiv preprint doi: https://doi.org/10.1101/077743; this version posted September 27, 2016. The copyright holder for this preprint (which was not certified by peer review) is the author/funder. All rights reserved. No reuse allowed without permission.



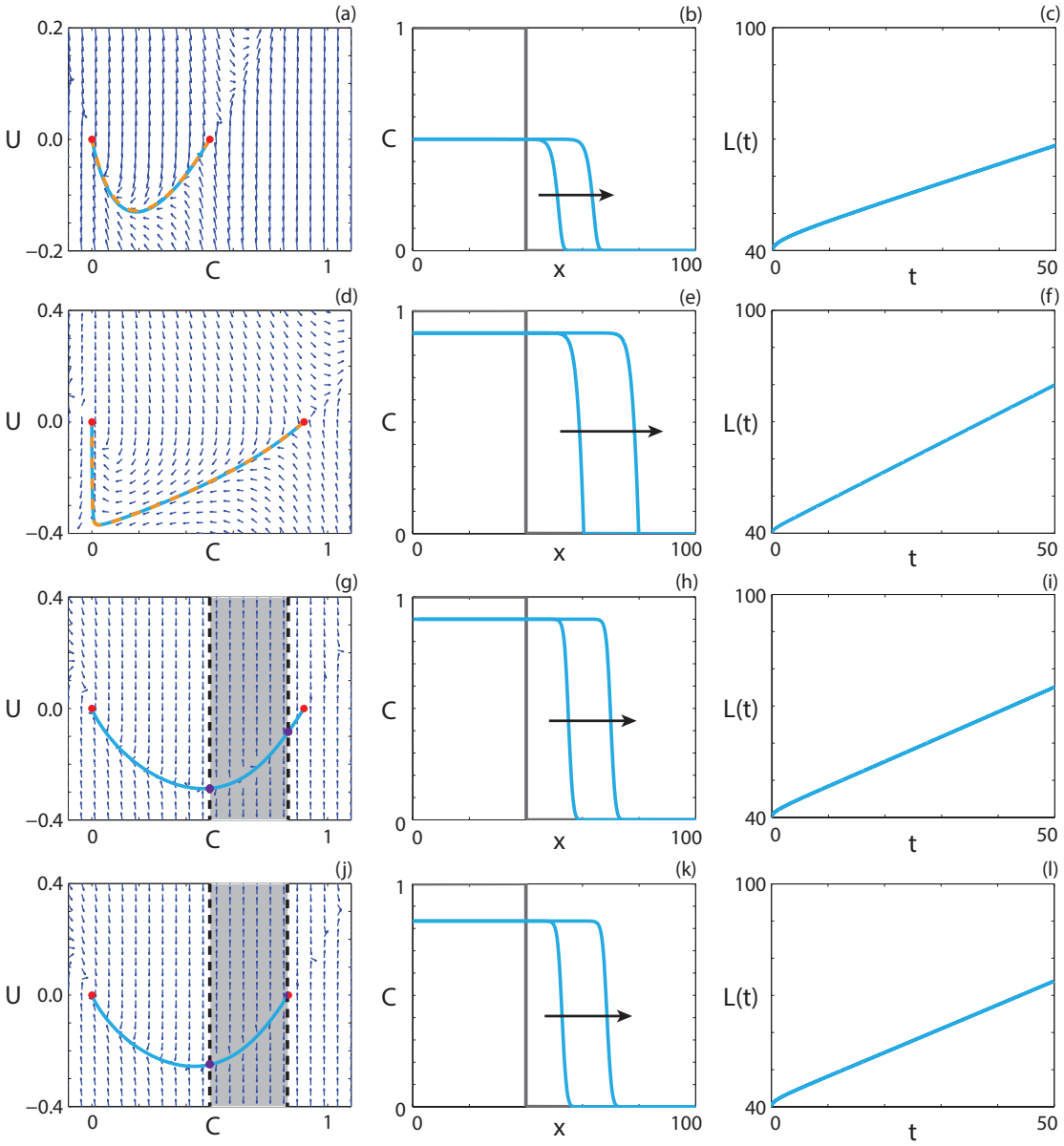


FIGURE 12. **Travelling wave behaviour for Equation** (33) **for various** $F_s(\overline{C})$. We consider (a)-(c) strictly positive $F_s(\overline{C})$ (Case 4.1), (d)-(f) extinction-degenerate non-negative $F_s(\overline{C})$ (Case 4.2), (g)-(i) positive-negative-positive $F(S\overline{C})$ (Case 4.3), and (j)-(l) capacity-degenerate positive-negative $F_s(\overline{C})$ (Case 4.4). (a), (d), (g), (j) Phase plane for the system (35)-(36) with the numerical solution of Equations (33) (cyan, solid) and (34) (orange, dashed), in $(C, U)$ co-ordinates, superimposed. The grey regions correspond to values of $\overline{C}$ where $F_s(\overline{C}) < 0$. The dashed black lines denote a wall of singularities. Red circles correspond to equilibrium points and purple circles correspond to holes in the wall. (b), (e), (h), (k) Numerical solution of Equation (33) at $t = 25$ and $t = 50$. The grey lines indicate the initial condition and the arrows indicate the direction of increasing time. (c), (f), (i), (l) The time evolution of the position of the leading edge of the travelling wave solution. Parameters used are (a)-(c) $P_m^i = 0.25$, $P_m^g = 0.5$, $P_p^i = P_p^g = 1$, $P_d^i = P_d^g = 0.5$, $v = 0.504$, (d)-(f) $P_m^i = 0$, $P_m^g = 1$, $P_p^i = P_p^g = 1$, $P_d^i = P_d^g = 0.1$, $v = 0.777$, (g)-(i) $P_m^i = 0.25$, $P_m^g = 0.05$, $P_p^i = P_p^g = 1$, $P_d^i = P_d^g = 0.1$, $v = 0.672$, (j)-(l) $P_m^i = 0.25$, $P_m^g = 0.05$, $P_p^i = P_p^g = 1$, $P_d^i = P_d^g = 1/6$, $v = 0.648$. All results are obtained using $\delta x = 0.1$, $\delta t = 0.01$, $\epsilon = 10^{-6}$.

bioRxiv preprint doi: https://doi.org/10.1101/077743; this version posted September 27, 2016. The copyright holder for this preprint (which was not certified by peer review) is the author/funder. All rights reserved. No reuse allowed without permission.



*Sub-case 4.3: Positive-negative-positive nonlinear diffusivity function.* For positive-negative-positive $F_s(\overline{C})$, the analysis in Case 2.3 holds provided that $\lambda > K$. Specifically, the minimum wave speed condition proved by Ferracuti *et al.* [36] implies that real-valued holes in the wall will be present for the scaled Fisher-Kolmogorov equation with $\lambda > K$. In turn, this suggests that the smooth travelling wave solutions passing through the region of negative diffusivity observed for Case 2.3 will be present with non-zero $K$. Travelling wave behaviour for Equation (33) with positive-negative-positive $F_s(\overline{C})$ is demonstrated in Figures 12(g)-(i). The travelling wave solution behaviour is similar to the behaviour in the corresponding case with $K = 0$ (Case 2.3), with the exception of the reduced carrying capacity.

*Sub-case 4.4: Capacity-degenerate positive-negative nonlinear diffusivity function.* The capacity-degenerate positive-negative diffusivity case, where $F_s(1) = R(S) = 0$, $F_s(\overline{C}) < 0$ for $\omega < \overline{C} < 1$ and $F_s(\overline{C}) \geq 0$ otherwise, might be thought to lead to travelling wave solutions with a sharp front near the carrying capacity density [38]. Similar to the approach for Case 2.4, we consider the conditions proposed by Maini *et al.* [38]. Again, we satisfy the condition that $F_s(1) = 0$. However, the minimum wave speed for the transformation of Equation (6) in $0 \leq \overline{C} < \omega$ is the same as the minimum wave speed for the transformation of Equation (6) in $\omega < \overline{C} \leq 1$. As such, we do not expect that Equation (33) will approach a travelling wave solution with a sharp front near $\overline{C} = 1$. We present travelling wave behaviour for Equation (33) with capacity-degenerate positive-negative $F_s(\overline{C})$ in Figures 12(j)-(l) and, as anticipated, observe that the travelling wave solution is a classic front.

*Sub-case 4.5: Positive-negative nonlinear diffusivity function.* The positive-negative case, where $F_s(\overline{C}) > 0$ for $0 \leq \overline{C} < \omega$ and $F_s(\overline{C}) < 0$ for $\omega < \overline{C} \leq 1$, cannot occur with $K = 0$. It is instructive to examine whether stable travelling wave solutions of Equation (33) exist, as the non-zero equilibrium point now occurs in the region where $F_s(\overline{C}) < 0$. If we perform standard linear analysis on Equations (35)-(36), the Jacobian at $(S, 0)$ has eigenvalues $\xi = (-v \pm \sqrt{v^2 + 4F(S)(\lambda(2S-1)+K)})/2F(S)$, which implies that the equilibrium point is an unstable node provided $v > 2\sqrt{-F(S)(\lambda(2S-1)+K)}$. The negative sign is present as $F(S) < 0$ for positive-negative $F_s(\overline{C})$. The Jacobian at $(0, 0)$ has eigenvalues $\xi = (-v \pm \sqrt{v^2 - 4D_i(\lambda - K)})/2D_i$, which is a stable node provided that $v > 2\sqrt{(\lambda - K)D_i}$. While there are infinitely many solution trajectories out of the unstable node, we require that the solution trajectory passes through the hole in the wall, and hence there is a single solution trajectory

bioRxiv preprint doi: https://doi.org/10.1101/077743; this version posted September 27, 2016. The copyright holder for this preprint (which was not certified by peer review) is the author/funder. All rights reserved. No reuse allowed without permission.



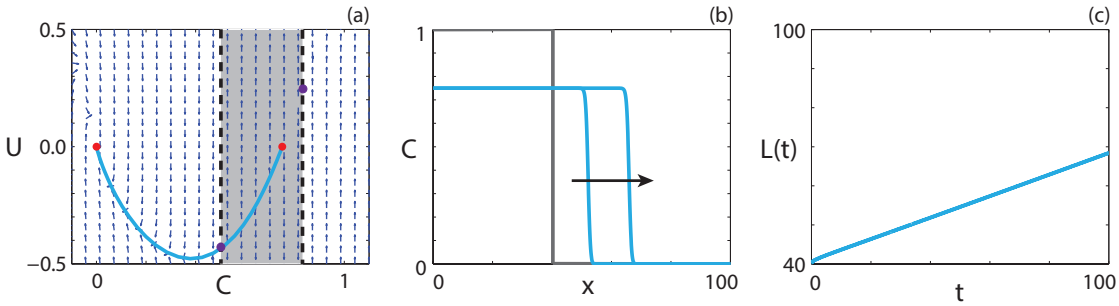


FIGURE 13. **Travelling wave behaviour for Equation** (33) **with positive-negative** $F_s(\overline{C})$ **(Case 4.5)**. (a) Phase plane for the system (35)-(36) with the numerical solution of Equation (33), in $(C, U)$ co-ordinates, superimposed. The grey region corresponds to values of $\overline{C}$ where $F_s(\overline{C}) < 0$. The dashed black lines denote a wall of singularities. Red circles correspond to equilibrium points and purple circles correspond to holes in the wall. (b) Numerical solution of Equation (33) at $t = 50$ and $t = 100$. The grey lines indicate the initial condition and the arrow indicates the direction of increasing time. (c) The time evolution of the position of the leading edge of the travelling wave solution. All results are obtained using $P_m^i = 0.05$, $P_m^g = 0.01$, $P_p^i = P_p^g = 1.0$, $P_d^i = P_d^g = 0.25$, $\delta x = 0.1$, $\delta t = 0.01$, $\epsilon = 10^{-6}$, $v = 0.2760$.

that forms a heteroclinic orbit.

Travelling wave behaviour for Equation (33) with positive-negative $F_s(\overline{C})$ is shown in Figure 13. The numerical solution of Equation (33), in $(C, U)$ co-ordinates, passes through the wall of singularities where Equation (36) is finite and forms a heteroclinic orbit between $(S, 0)$ and $(0, 0)$. The travelling wave front is of classic type, a result predicted by the analysis performed by Maini *et al.* [38] as $F_s(0) \neq 0$ and $F_s(1) \neq 0$.

**Case 5: Equal motility rates, no grouped agent death.** Results in Figure 1(g)-(h) indicate that restricting death events to isolated agents significantly change the behaviour of the agent population. This represents a co-operative mechanism, as there is a benefit to being in close proximity to another agent. In the case where $P_d^i \neq 0$ and $P_d^g = 0$, the source term can be expressed as an Allee effect [15]

$$R(C) = rC(1 - C)(C - A), \tag{43}$$

where

$$r = K_i - \lambda_i + \lambda_g, \tag{44}$$

bioRxiv preprint doi: https://doi.org/10.1101/077743; this version posted September 27, 2016. The copyright holder for this preprint (which was not certified by peer review) is the author/funder. All rights reserved. No reuse allowed without permission.



is the intrinsic growth rate, and

$$A = \frac{K_i - \lambda_i}{K_i - \lambda_i + \lambda_g}, \tag{45}$$

is the Allee parameter. It follows that Equation (1) becomes

$$\frac{\partial C}{\partial t} = D\frac{\partial^2 C}{\partial x^2} + (K_i - \lambda_i + \lambda_g)C(1-C)\left(C - \frac{K_i - \lambda_i}{K_i - \lambda_i + \lambda_g}\right). \tag{46}$$

If $K_i > \lambda_i$, $R(C)$ represents the strong Allee effect, $A > 0$ [15]. The strong Allee effect has bistable growth kinetics, namely, $R(C) < 0$ for $0 < C < A$ and $R(C) > 0$ for $A < C < 1$. For low densities there are significantly more isolated agents than grouped agents, which corresponds to negative growth if $K_i > \lambda_i$. If $\lambda_i > K_i$, and $\lambda_g > 0$, $R(C) > 0$ for $0 < C < 1$. There are two possibilities for this case: $r > 0$ and $r < 0$. If $r > 0$ then $A < 0$ and hence the growth rate is inhibited at low density, but remains positive, which corresponds to the weak Allee effect [15]. For the case where $r < 0$ and $R(C) > 0$, we obtain $A > 1$ for all parameter combinations. Interestingly, this implies that the growth rate is inhibited at high density, but remains positive. This situation does not correspond to either the weak or strong Allee effect, and we term this behaviour the reverse Allee effect. It is not possible to have a combination of parameters that results in $r < 0$ and $0 < A < 1$ as all of our parameters are non-negative. Representative source terms showing the three types of Allee effect are compared with a logistic source term in Figure 14.

For $P_m^i = P_m^g$, we have linear diffusion in Equation (46). Reaction-diffusion equations with linear diffusion and either weak or strong Allee kinetics have been well-studied [15,19,22,23,25,26,28,30]. We briefly present results here and interpret these in the context of examining the long time travelling wave solution. For additional details we refer the reader to [15]. We look for solutions in the travelling wave co-ordinate $z = x - vt$. The existence of such solutions has been examined previously and requirements for the initial conditions to converge to a travelling wave solution have been found for both the case where $A < 0$ and where $0 < A < 1$ [23]. Transforming Equation (46) into travelling wave co-ordinates we obtain

$$D\frac{\mathrm{d}^2 C}{\mathrm{d}z^2} + v\frac{\mathrm{d}C}{\mathrm{d}z} + (K_i - \lambda_i + \lambda_g)C(1-C)\left(C - \frac{K_i - \lambda_i}{K_i - \lambda_i + \lambda_g}\right) = 0, \ -\infty < z < \infty, \tag{47}$$

where $D = D_g = D_i$. If $U = \mathrm{d}C/\mathrm{d}z$, Equation (47) can be expressed as

$$\frac{\mathrm{d}C}{\mathrm{d}z} = U, \tag{48}$$

$$\frac{\mathrm{d}U}{\mathrm{d}z} = \frac{-vU}{D} - \frac{(K_i - \lambda_i + \lambda_g)C(1-C)(C-A)}{D}. \tag{49}$$

bioRxiv preprint doi: https://doi.org/10.1101/077743; this version posted September 27, 2016. The copyright holder for this preprint (which was not certified by peer review) is the author/funder. All rights reserved. No reuse allowed without permission.



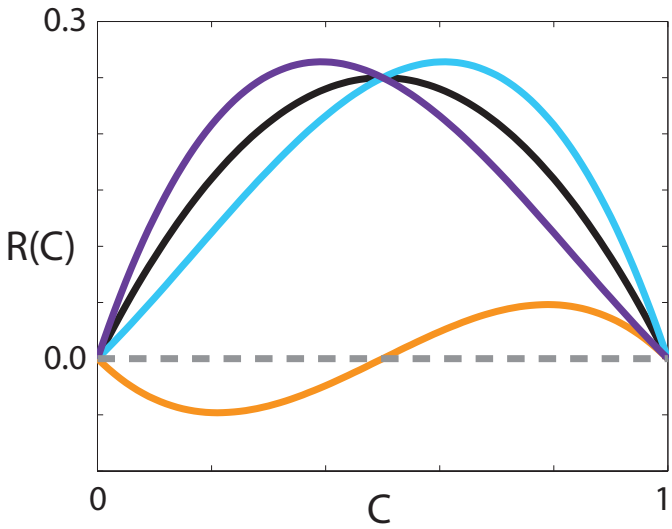


FIGURE 14. **Comparison of source terms**. $R(C)$ corresponding to the weak Allee effect with $r = 1$, $A = -0.5$ (cyan), strong Allee effect with $r = 1$, $A = 0.5$ (orange), reverse Allee effect with $r = -1$, $A = 1.5$ (purple) and logistic growth with $r = 1$ (black).

This system of equations has three equilibrium points: $(C, U) = (0, 0)$; $(C, U) = (1, 0)$; and $(C, U) = (A, 0)$. We are only concerned with physically relevant equilibrium points, where $0 \leq C \leq 1$. If $A < 0$ or $A > 1$, there are only two physically relevant equilibrium points as the equilibrium point at $(C, U) = (A, 0)$ has no physical meaning. Performing standard linear stability analysis by examining the eigenvalues of Jacobian of the system, the characteristic equation at $(0, 0)$ has solutions $\xi = (-v \pm \sqrt{v^2 + 4(K_i - \lambda_i)D})/2D$, which implies that the equilibrium point is a stable node when $\lambda_i > K_i$, provided the wave speed satisfies $v > 2\sqrt{(\lambda_i - K_i)D}$. If the wave speed does not satisfy this condition then the equilibrium point is a stable spiral, which implies that the heteroclinic orbit enters non-physical values of $C$. If $K_i > \lambda_i$, $(0, 0)$ is a saddle point. The characteristic equation for the equilibrium point at $(1, 0)$ has solutions $\xi = (-v \pm \sqrt{v^2 + 4\lambda_g D})/2D$, which implies that the equilibrium point is a saddle point, as $\lambda_g$ is non-negative. A heteroclinic orbit between $(1, 0)$ and $(0, 0)$ exists for a unique wave speed [25]. The equilibrium point at $(A, 0)$ has a characteristic equation with solutions $\xi = (-v \pm \sqrt{v^2 - 4\lambda_g AD})/2D$. As we are only concerned with physically realistic equilibrium points, that is, where $0 < A < 1$, the equilibrium point $(A, 0)$ will be a stable node provided that the minimum wave speed $v > 2\sqrt{\lambda_g AD}$ is satisfied, and a stable spiral otherwise. The spiral behaviour does not cause the solution trajectory to become non-physical and hence this wave

bioRxiv preprint doi: https://doi.org/10.1101/077743; this version posted September 27, 2016. The copyright holder for this preprint (which was not certified by peer review) is the author/funder. All rights reserved. No reuse allowed without permission.



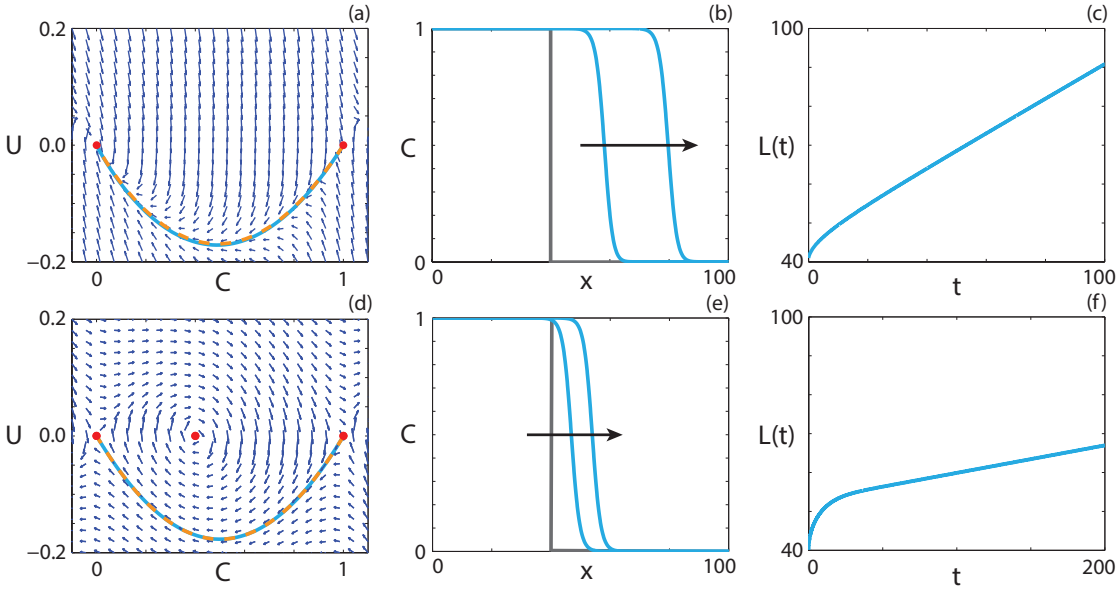


FIGURE 15. **Travelling wave behaviour for the (a)-(c) weak Allee effect and the (d)-(f) strong Allee effect with a constant $F(C)$ (Case 5).** (a), (d) Phase plane for the system (48)-(49) with the numerical solution of Equations (46) (cyan, solid) and (47) (orange, dashed), in $(C, U)$ co-ordinates, superimposed. Red circles correspond to equilibrium points. (b), (e) Numerical solution of Equation (46) calculated at (b) $t = 50$ and $t = 100$, (e) $t = 100$ and $t = 200$. The grey lines indicate the initial condition and the arrows indicate the direction of increasing time. (c), (f) The time evolution of $L(t)$. All results are obtained with $\delta x = 0.1$, $\delta t = 0.01$, $\epsilon = 10^{-6}$, $P_d^g = 0$, (a)-(c) $P_m^i = 0.5$, $P_m^g = 0.5$, $P_p^i = 0.7$, $P_p^g = 0.4$, $P_d^i = 0.5$, $v = 0.44$, (d)-(f) $P_m^i = 1.0$, $P_m^g = 1.0$, $P_p^i = 0.3$, $P_p^g = 0.3$, $P_d^i = 0.5$, $v = 0.072$.

speed condition is not required to obtain physically meaningful solutions.

Solutions that display travelling wave behaviour for the weak Allee effect are presented in Figures 15(a)-(c). There is a heteroclinic solution trajectory for Equations (48)-(49) between the two equilibrium points, and the numerical solution of Equation (46) matches the solution trajectory in $(C, U)$ co-ordinates. The results in Figures 15(b)-(c) suggest that the numerical solution of Equation (46) with the weak Allee effect approaches a travelling wave solution. Since the source term for the reverse Allee effect is qualitatively similar to the weak Allee effect, we do not present solutions here. Solution behaviour for the reverse Allee effect can be found in the Supplementary Material.

bioRxiv preprint doi: https://doi.org/10.1101/077743; this version posted September 27, 2016. The copyright holder for this preprint (which was not certified by peer review) is the author/funder. All rights reserved. No reuse allowed without permission.



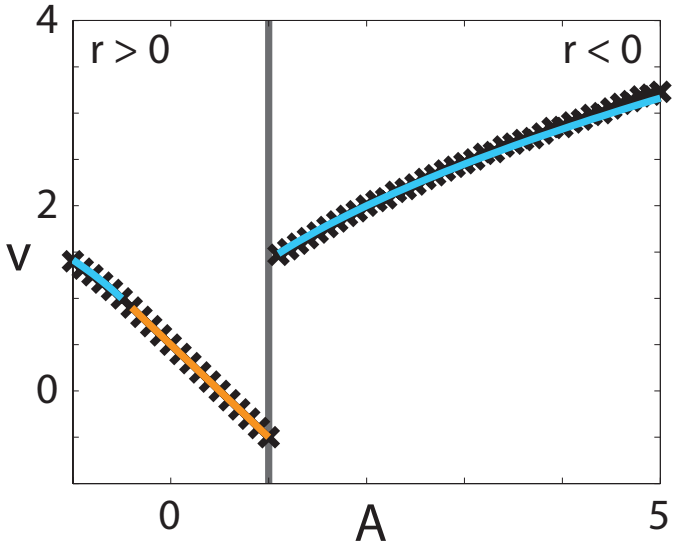


FIGURE 16. **Wave speed comparison for Case 5**. Comparison of observed wave speeds obtained from the numerical solution of Equation (46). For $A \leq 1$ results are obtained using $r = 1$, whereas for $A > 1$ results are obtained using $r = -1$. The cyan line corresponds to $v = 2\sqrt{-ArD}$ and the orange line corresponds to $v = 2\sqrt{rD}(1/2 - A)$.

A travelling wave solution of Equation (46) in a parameter regime that results in a strong Allee effect is now considered. The phase plane for Equations (48)-(49), presented in Figure 15(d), has three physically meaningful equilibrium points, and the equilibrium point at $(0, 0)$ is unstable, unlike in Figure 15(d). However, there is still a heteroclinic orbit between $(1, 0)$ and $(0, 0)$. Unlike for the weak Allee effect, the wave speed that admits this solution trajectory is unique [25]. The numerical solution of Equation (46) shows the solution approaches a travelling wave, although the approach is slower than for the weak Allee effect. This is intuitive, as the growth rate for the weak Allee effect is non-negative, while the strong Allee effect has regions of negative growth.

It is instructive to consider how $v$ depends on $A$. We calculate the numerical solution of Equation (46) for a range of $A$ values with $r = 1$ for $A \leq 1$, and $r = -1$ for $A > 1$, and use the numerical solution to calculate $v$ at sufficiently late time. We consider $r < 0$ for $A > 1$ because, due to our parameters being non-negative, $A < 1$ for $r > 0$. The minimum wave speed for the travelling wave solution is known for $A \leq 0$, namely, $v^* = 2\sqrt{-ArD}$ for $A \leq -1/2$ and $v^* = 2\sqrt{rD}(1/2-A)$ for $-1/2 \leq A \leq 0$ [28]. For $0 < A < 1$ there is a unique wave speed, $v = \sqrt{2rD}(1/2 - A)$ [28]. Consequently, for $A > 1/2$, the population will tend to extinction because the travelling wave

bioRxiv preprint doi: https://doi.org/10.1101/077743; this version posted September 27, 2016. The copyright holder for this preprint (which was not certified by peer review) is the author/funder. All rights reserved. No reuse allowed without permission.



speed is negative [28]. For the case where $A > 1$ it is unclear whether there is a minimum wave speed condition. A comparison between the observed wave speed for each $A$ value and the predicted minimum wave speed is given in Figure 16. The predicted wave speeds match the observed wave speeds well for $A \leq 1$. For $A > 1$ we superimpose the wave speed prediction $v = 2\sqrt{-ArD}$, and observe that the predictions match the numerical wave speeds well. For the case $A > 1$ we require that $\lambda_i > K_i$, and hence the minimum wave speed condition is the same as for the weak Allee effect.

**Case 6: Different motility rates, no grouped agent death.** For $P_m^i \neq P_m^g$ and $P_d^g = 0$, there is a co-operative mechanism in terms of increased survival for agents in close proximity to other agents. In this parameter regime Equation (1) becomes

$$\frac{\partial C}{\partial t} = \frac{\partial}{\partial x}\left(F(C)\frac{\partial C}{\partial x}\right) + (K_i - \lambda_i + \lambda_g)C(1-C)\left(C - \frac{K_i - \lambda_i}{K_i - \lambda_i + \lambda_g}\right), \tag{50}$$

where $F(C) = D_i(1-4C+3C^2)+D_g(4C-3C^2)$. Note that $F(C)$ is the same as in Case 2 and, as such, encodes the same four types of qualitative behaviour. To examine the long term travelling wave behaviour of Equation (50), we transform Equation (50) into travelling wave co-ordinates, $z = x - vt$, giving

$$v\frac{\mathrm{d}C}{\mathrm{d}z} + F(C)\frac{\mathrm{d}^2C}{\mathrm{d}z^2} + (D_i - D_g)(6C-4)\left(\frac{\mathrm{d}C}{\mathrm{d}z}\right)^2 + R(C) = 0, \ -\infty < z < \infty, \tag{51}$$

where $R(C) = (K_i - \lambda_i + \lambda_g)C(1-C)(C - (K_i - \lambda_i)/(K_i - \lambda_i + \lambda_g))$. Making the substitution $U = \mathrm{d}C/\mathrm{d}z$ results in

$$\frac{\mathrm{d}C}{\mathrm{d}z} = U, \tag{52}$$

$$\frac{\mathrm{d}U}{\mathrm{d}z} = \frac{-vU - (D_i - D_g)(6C-4)U^2(K_i - \lambda_i + \lambda_g) - R(C))}{F(C)}. \tag{53}$$

Equation (53) is singular if $F(C) = 0$ for $0 \leq C \leq 1$. It is therefore of interest to determine whether travelling wave solutions can be found for each class of $F(C)$.

*Sub-case 6.1: Strictly positive nonlinear diffusivity function.* Strictly positive $F(C)$ corresponds to parameters in the grey region of Figure 3(a). As the wave speed for an arbitrary $A$ is not determined by linear analysis for the Allee equation with constant diffusivity, we follow the approach of Hadeler [42–44] to determine a condition for $v > 0$. Making the transformation

$$\hat{z} = \int_0^z \frac{1}{D_i(1 - 4C(s) + 3C(s)^2) + D_g(4C(s) - 3C(s)^2)}\,\mathrm{d}s, \tag{54}$$

bioRxiv preprint doi: https://doi.org/10.1101/077743; this version posted September 27, 2016. The copyright holder for this preprint (which was not certified by peer review) is the author/funder. All rights reserved. No reuse allowed without permission.



results in

$$\frac{\mathrm{d}C}{\mathrm{d}\hat{z}} = \hat{U}, \tag{55}$$

$$\frac{\mathrm{d}\hat{U}}{\mathrm{d}\hat{z}} = -v\hat{U} - \lambda\Big(D_i(1-4C+3C^2) + D_g(4C-3C^2)\Big)(K_i-\lambda_i+\lambda_g)C(1-C)\left(C - \frac{K_i-\lambda_i}{K_i-\lambda_i+\lambda_g}\right). \tag{56}$$

For $v > 0$ we require that the transformed source term is, on average, positive, which corresponds to [42–45]

$$\int_0^1 (K_i-\lambda_i+\lambda_g)\Big(D_i\big(1-4C+3C^2\big)+D_g\big(4C-3C^2\big)\Big)C(1-C)\left(C-\frac{K_i-\lambda_i}{K_i-\lambda_i+\lambda_g}\right)\mathrm{d}C > 0. \tag{57}$$

Condition (57) is equivalent to

$$(6\lambda_g - 5K_i + 5\lambda_i)D_g - \lambda_g D_i > 0. \tag{58}$$

For the case with $r > 0$, Condition (58) is equivalent to $(A-1)D_i + (6-11A)D_g > 0$. Since $D_i < 4D_g$ for $F(C) > 0$ on $0 \leq C \leq 1$, it is trivial to see that for $A < 0$, $v > 0$. Interestingly, for $A > 0$, the threshold $A$ value for the population to persist increases if $P_m^g > P_m^i$, and decreases otherwise. For example, if $P_m^i = 0$ then $A < 6/11$ leads to persistence, higher than the threshold $A$ value in the case with constant $F(C)$. Alternatively, as $P_m^i \to 4P_m^g$, $A \to 2/7$. This implies that populations where isolated agents are significantly more motile than grouped agents are more susceptible to extinction. This result is intuitive, as the parameter regime considered here describes a co-operative benefit, namely, a reduced death rate for agents in close proximity to other agents. Finally, for the reverse Allee case, where $r < 0$ and $A > 1$, Condition (58) is always satisfied and the population persists.

Travelling wave solutions for the strong Allee effect with a strictly positive $F(C)$ are shown in Figure 17. For the strong Allee effect, with parameters that correspond to $A = 1/4$, presented in Figures 17(a)-(c), we observe a heteroclinic orbit between $(1,0)$ and $(0,0)$. The numerical solution of Equation (50) in this parameter regime approaches a travelling wave solution with $v > 0$. However, if we consider a parameter regime that corresponds to the strong Allee effect with $A = 4/9$, presented in Figures 17(d)-(f), we observe that, while a heteroclinic orbit between $(1,0)$ and $(0,0)$ exists, it corresponds to a negative wave speed. As a consequence, the population tends to extinction in a birth/death parameter regime that would otherwise result in the persistence of the population if the diffusivity is constant. As both the weak and reverse Allee effect are

bioRxiv preprint doi: https://doi.org/10.1101/077743; this version posted September 27, 2016. The copyright holder for this preprint (which was not certified by peer review) is the author/funder. All rights reserved. No reuse allowed without permission.



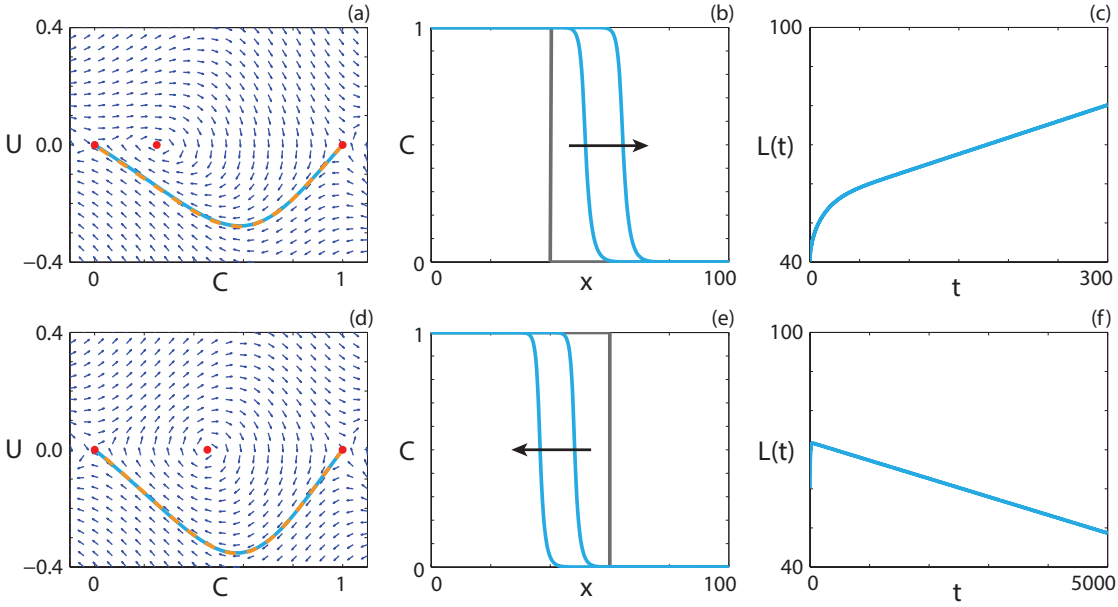


FIGURE 17. **Travelling wave behaviour for the Equation** (50) **with the strong Allee effect and strictly positive** $F(C)$ **(Case 6.1)**. (a), (d) Phase plane for the system (52)-(53) with the numerical solution of Equations (50) (cyan, solid) and (51) (orange, dashed), in $(C, U)$ co-ordinates, superimposed. Red circles correspond to equilibrium points. (b), (e) Numerical solution of Equation (50) calculated at (b) $= 150$ and $t = 300$, (e) $t = 2500$ and $t = 5000$. The grey lines indicate the initial condition and the arrows indicate the direction of increasing time. (c), (f) The time evolution of $L(t)$. All results are obtained with $\delta x = 0.1$, $\delta t = 0.01$, $\epsilon = 10^{-6}$, $P_d^g = 0$, (a)-(c) $P_m^i = 1.0$, $P_m^g = 0.5$, $P_p^i = 0.4$, $P_p^g = 0.3$, $P_d^i = 0.5$, $v = 0.084$, (d)-(f) $P_m^i = 1.0$, $P_m^g = 0.5$, $P_p^i = 0.4$, $P_p^g = 0.3$, $P_d^i = 0.65$, $v = -0.004$.

qualitatively similar to Fisher kinetics, numerical solutions are not presented here. Numerical solutions can be found in the Supplementary Material.

*Sub-case 6.2: Extinction-degenerate non-negative nonlinear diffusivity function.* The case where $F(0) = 0$ corresponds to parameters along the orange line in Figure 3(a). Sánchez-Garduño and Maini [41] demonstrate that Condition (57) must be satisfied for travelling wave solutions to have $v > 0$. Furthermore, there is a critical wave speed that results in a sharp-fronted travelling wave [41]. From the results obtained for Case 6.1, Condition (57) is always satisfied for $A < 0$ or $A > 1$. For parameter regimes where $0 < A < 1$ the choice of $P_m^i$ and $P_m^g$ influences whether Condition (57) is satisfied. To obtain an extinction-degenerate diffusivity we require that $P_m^i = 0$. Hence (58) implies that for $A < 6/11$ the wave speed will be positive. To obtain a

bioRxiv preprint doi: https://doi.org/10.1101/077743; this version posted September 27, 2016. The copyright holder for this preprint (which was not certified by peer review) is the author/funder. All rights reserved. No reuse allowed without permission.



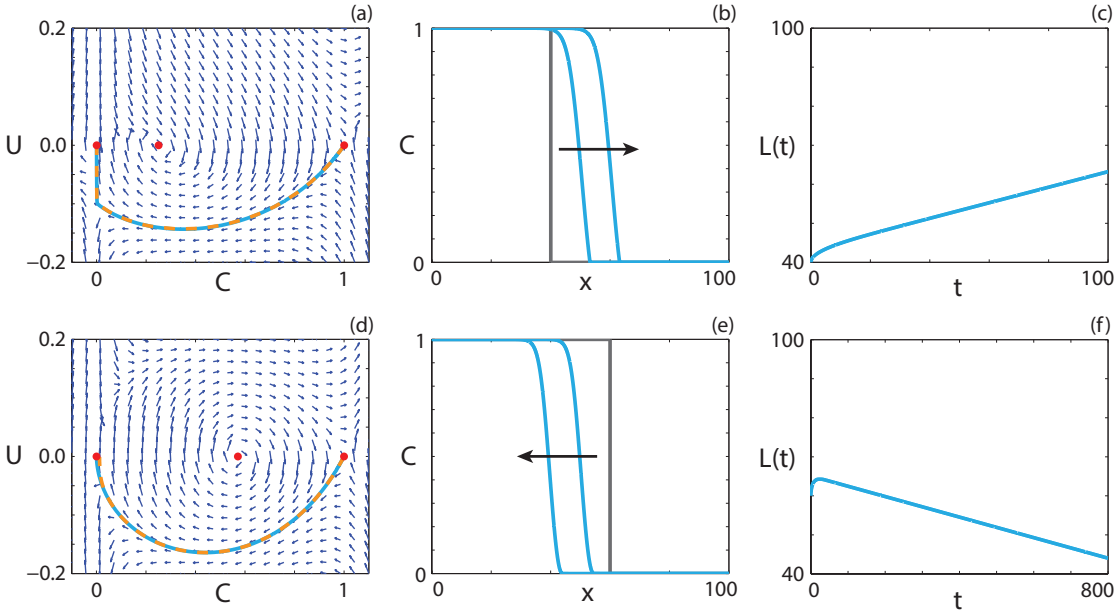


FIGURE 18. **Travelling wave behaviour for Equation** (50) **with the strong Allee effect and extinction-degenerate non-negative** $F(C)$ **(Case 6.2)**. (a), (d) Phase plane for the system (52)-(53) with the numerical solution of Equations (50) (cyan, solid) and (51) (orange, dashed), in $(C, U)$ co-ordinates, superimposed. Red circles correspond to equilibrium points. (b), (e) Numerical solution of Equation (50) calculated at (b) $t = 50$ and $t = 100$, (e) $t = 400$ and $t = 800$. The grey lines indicate the initial condition and the arrows indicate the direction of increasing time. (c), (f) The time evolution of $L(t)$. All results are obtained with $\delta x = 0.01$, $\delta t = 0.005$, $\epsilon = 10^{-6}$, $P_m^i = 0$, $P_m^g = 1.0$,$P_d^g = 0$, (a)-(c) $P_p^i = 0.4$, $P_p^g = 0.3$, $P_d^i = 0.5$, $v = 0.199$, (d)-(f) $P_p^i = 0.4$, $P_p^g = 0.3$, $P_d^i = 0.8$, $v = -0.026$.

positive wave speed with constant $F(C)$, we require $A < 1/2$, which implies that the population is more likely to persist in an parameter regime that leads to extinction-degenerate non-negative $F(C)$.

Travelling wave behaviour for the strong Allee effect with extinction-degenerate non-negative $F(C)$ is shown in Figure 18. The numerical solution of Equation (50) with $A = 1/4$, in Figures 18(a)-(c), leads to a sharp-fronted travelling wave solution near $C = 0$ with $v > 0$. With $A = 1/4$, we expect to obtain $v > 0$. For a parameter regime that results in $A = 4/7$, we obtain a travelling wave solution of Equation (50) with $v < 0$ (Figures 18(d)-(f)). Interestingly, the sharp front near $C = 0$ is not present for the strong Allee effect with $v < 0$, unlike with $v > 0$, where the wave front is smooth.

bioRxiv preprint doi: https://doi.org/10.1101/077743; this version posted September 27, 2016. The copyright holder for this preprint (which was not certified by peer review) is the author/funder. All rights reserved. No reuse allowed without permission.



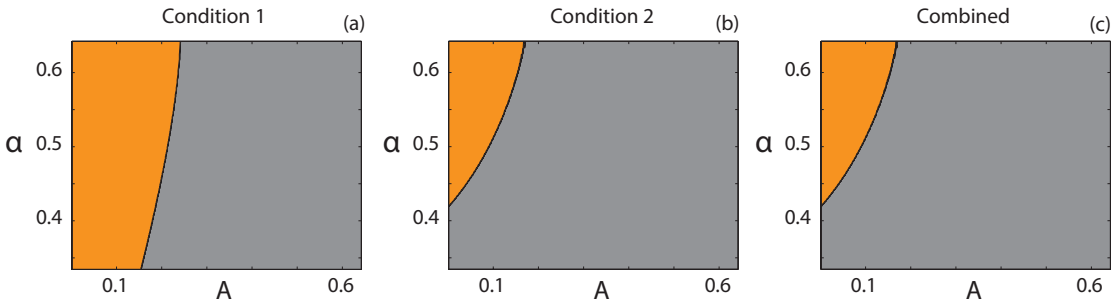


FIGURE 19. **Parameter pairs that satisfy Kuzmin and Ruggerini's Conditions**. (a) Condition (59), (b) Condition (60), (c) Conditions (59)-(60) combined. Orange regions correspond to parameter pairs that satisfy the respective condition(s), whereas grey regions correspond to parameter pairs that do not.

*Sub-case 6.3: Positive-negative-positive nonlinear diffusivity function.* A positive-negative-positive $F(C)$, where there is an interval $\alpha < C < \beta$ where $F(C) < 0$, corresponds to parameter pairs highlighted in purple in Figure 3(a). Kuzmin and Ruggerini [37] examine reaction-diffusion equations with similar properties for the strong Allee effect, in the context of diffusion-aggregation models, and provide conditions for smooth travelling wave solutions to exist. For a solution with $v > 0$, we require $A < \alpha$ [37] and

$$\int_0^\alpha F(C)R(C)\ \mathrm{d}C > 0. \tag{59}$$

Furthermore, we require [37]

$$3\int_0^\alpha F(C)R(C)\ \mathrm{d}C \geq \max\{\Phi(\sigma), \Phi(\rho)\}, \tag{60}$$

where

$$\Phi(y) = 8\alpha^2 y + 4\sqrt{4\alpha^2 y^2 - 2m\alpha^3 y},$$
$$\sigma = \sup_{C\in[\alpha,\beta)}\left[\frac{F(C)R(C)}{C-\beta}\right],\ \rho = \sup_{C\in(\beta,1]}\left[\frac{F(C)R(C)}{C-\beta}\right],\ \text{and}$$
$$m = \min_{C\in[0,A]}\left[F(C)R(C)\right].$$

A suite of $P_m^g$ values with $P_m^i = 1$, which correspond to $1/3 < \alpha < 2/3$ are considered for parameter regimes that result in $A < \alpha$. Figures 19(a)-(c) show the parameter spaces, $(A, \alpha)$, that satisfy Condition (59), Condition (60) and Conditions (59)-(60) simultaneously, respectively. Orange reFgions represent parameter pairs where the condition is satisfied and grey regions represent parameter pairs where the condition is not satisfied. These results suggest that smooth travelling

bioRxiv preprint doi: https://doi.org/10.1101/077743; this version posted September 27, 2016. The copyright holder for this preprint (which was not certified by peer review) is the author/funder. All rights reserved. No reuse allowed without permission.



wave solutions should exist for certain choices of parameters. Interestingly, all parameter pairs that satisfy Condition (59) also satisfy Condition (60).

For Case 2.3 and Case 4.3, smooth travelling wave solutions that pass through holes in the wall of singularities for positive-negative-positive $F(C)$ are obtained. The minimum wave speed bound presented by Ferracuti *et al.* [36] implies that the location of the holes in the wall occur are real-valued for the wave speed arising from the Heaviside initial condition. As such, to obtain smooth travelling wave solutions of Equation (50) with positive-negative-positive $F(C)$, we might expect that the wave speed satisfies $v > 2\sqrt{F'(\beta)R(\beta)}$, such that the holes in the wall at $C = \beta$ are real-valued.

Following the approach used for Case 2.3, it is simple to demonstrate that both the weak and reverse Allee effect have real-valued holes in the wall. As such, we observe heteroclinic orbits between $(1, 0)$ and $(0, 0)$ that pass through the holes in the wall, and present the corresponding travelling wave solutions in the Supplementary Material. We now examine numerical solutions of Equation (50) with the strong Allee effect. For parameter regimes that give rise to wave speeds that satisfy $v > 2\sqrt{F'(\beta)R(\beta)}$, numerical travelling wave solutions could not be found. While the condition for real-valued holes in the wall is satisfied, the zeros of Equation (53) are imaginary for a certain interval of $C > \beta$. This corresponds to a nullcline that is not real-valued for certain $C$ values.

We now consider parameter regimes corresponding to the strong Allee effect with the additional restriction that $v < 2\sqrt{F'(C)R(C)}$ for $2/3 < C \leq 1$. For all $P_m^i$ and $P_m^g$ that give rise to a positive-negative-positive $F(C)$, holes in the wall at $C = \beta$ do not exist and, as such, we do not expect to obtain smooth solutions. Interestingly, we observe travelling wave solutions with shocks such that the solution never enters the region $\alpha < C < \beta$. An example of a shock-fronted travelling wave solution for the strong Allee effect with both $v > 0$ and $v < 0$ is shown in Figures 20(a)-(c) and Figures 20(d)-(f), respectively. Solutions of diffusion equations, without any source terms, that contain shocks have been reported previously [50, 51]. Similarly, shock-fronted travelling wave solutions arise in other kinds of models, including multispecies models of combustion [54] and haptotactic cell migration [53]. However, the models presented here are

bioRxiv preprint doi: https://doi.org/10.1101/077743; this version posted September 27, 2016. The copyright holder for this preprint (which was not certified by peer review) is the author/funder. All rights reserved. No reuse allowed without permission.



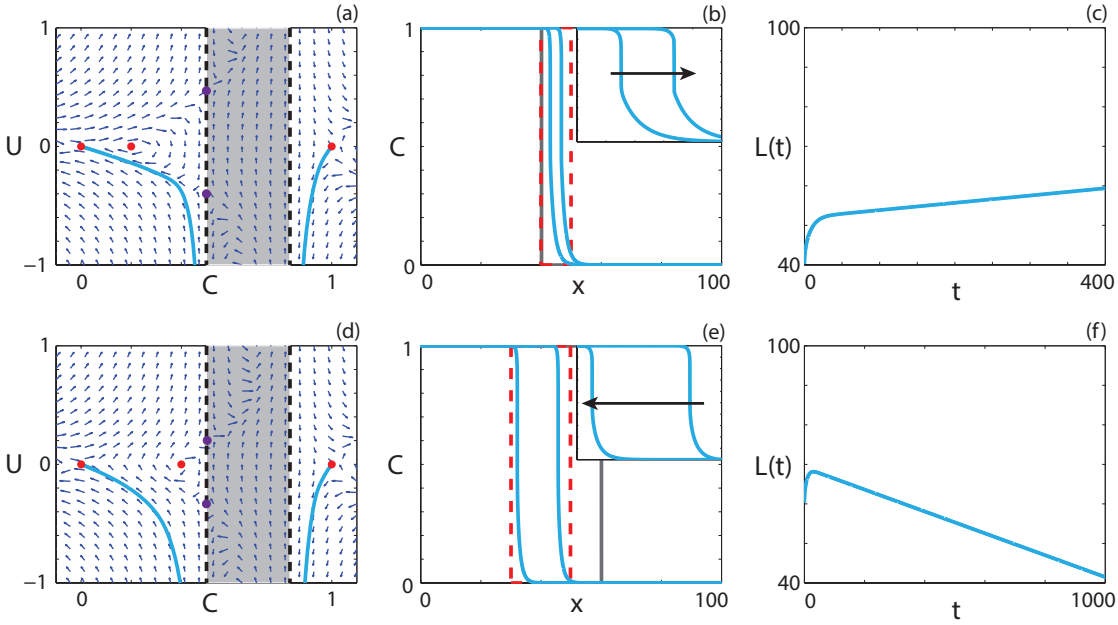


FIGURE 20. **Travelling wave behaviour for Equation** (50) **with the strong Allee effect and positive-negative-positive** $F(C)$ **(Case 6.3)**. (a), (d) Phase plane for the system (52)-(53) with the numerical solution of Equation (50) (cyan, solid), in $(C, U)$ co-ordinates, superimposed. The dashed black lines denote a wall of singularities. Red circles correspond to equilibrium points and purple circles correspond to holes in the wall. (b), (e) Numerical solution of Equation (50) calculated at (b) $t = 200$ and $t = 400$, (e) $t = 500$ and $t = 1000$. The grey lines indicate the initial condition and the arrows indicate the direction of increasing time. The insets correspond to the areas within the red dashed lines, and highlight the shocks. (c), (f) The time evolution of $L(t)$. All results are obtained with $\delta x = 0.1$, $\delta t = 0.01$, $\epsilon = 10^{-6}$, $P_d^g = 0$, (a)-(c) $P_m^i = 0.5$, $P_m^g = 0.1$, $P_p^i = 0.5$, $P_p^g = 0.4$, $P_d^i = 0.6$, $v = 0.009$, (d)-(f) $P_m^i = 0.5$, $P_m^g = 0.1$, $P_p^i = 0.4$, $P_p^g = 0.2$, $P_d^i = 0.5$, $v = -0.028$.

very different, and it is therefore of interest to determine the properties of the reaction-diffusion equation that lead to shock-fronted travelling wave solutions.

*Sub-case 4: Capacity-degenerate positive-negative nonlinear diffusivity function.* Capacity-degenerate positive-negative $F(C)$, where $F(1) = 0$, arises if $P_m^g = 0$ and includes an interval $1/3 < C < 1$ where $F(C) < 0$. For Case 2.4, despite the degenerate nature of the nonlinear diffusivity function at $C = 1$, we did not obtain solutions with a sharp front near $C = 1$. Instead, the solution passes through the region of negative diffusivity and a hole in the wall at $C = 1/3$ , leading to smooth travelling wave solutions. As such, we expect similar solutions for both the weak and reverse Allee effect due to the qualitatively similar behaviour of the $R(C)$ function. It is of interest to

bioRxiv preprint doi: https://doi.org/10.1101/077743; this version posted September 27, 2016. The copyright holder for this preprint (which was not certified by peer review) is the author/funder. All rights reserved. No reuse allowed without permission.



examine whether smooth or shock-fronted travelling wave solutions arise from Equation (50) for the strong Allee effect, as for the positive-negative-positive diffusivity examined for Case 6.3 no smooth travelling wave solutions could be found.

As expected, smooth travelling wave solutions for both the weak and reverse Allee effects with capacity-degenerate positive-negative $F(C)$ are obtained. The solution behaviour for both the weak and reverse Allee effects are presented in the Supplementary Material. For the strong Allee effect, we examine a considerable number of parameter regimes and initial conditions and are unable to find travelling wave solutions.

**Case 7: Equal motility rates, different death rates.** Without the restriction that only isolated agents are able to undergo death events ($P_d^g \neq 0$), death events can be considered as either a co-operative mechanism ($P_d^i > P_d^g$), such as group defence against predation, or a competitive mechanism ($P_d^i < P_d^g$), where a population is more easily discovered and eradicated, compared to an isolated individual. In these parameter regimes, Equation (1) can be expressed as

$$\frac{\partial C}{\partial t} = D\frac{\partial^2 C}{\partial x^2} + (K_i - K_g - \lambda_i + \lambda_g)A_1 C\left(1 - \frac{C}{A_1}\right)\left(C - A_2\right), \tag{61}$$

where

$$A_1 = \frac{2\lambda_i - \lambda - 2K_i + 2K_g - \sqrt{\lambda_g^2 + 4K_g(\lambda_i - \lambda_g - K_i + K_g)}}{2(\lambda_i - \lambda_g - K_i + K_g)},$$
$$A_2 = \frac{2\lambda_i - \lambda - 2K_i + 2K_g + \sqrt{\lambda_g^2 + 4K_g(\lambda_i - \lambda_g - K_i + K_g)}}{2(\lambda_i - \lambda_g - K_i + K_g)}, \tag{62}$$

provided that $\lambda_g \geq 2(K_g + \sqrt{Kg(K_i - \lambda_i)})$ or $\lambda_i > K_i$. If this is not satisfied, $R(C) \leq 0$ for $0 \leq C \leq 1$ and the population will tend to extinction. The corresponding ODE in travelling wave co-ordinates is

$$v\frac{\mathrm{d}C}{\mathrm{d}z} + D\frac{\mathrm{d}^2 C}{\mathrm{d}z^2} + (K_i - K_g - \lambda_i + \lambda_g)A_1 C\left(1 - \frac{C}{A_1}\right)\left(C - A_2\right) = 0, \quad -\infty < z < \infty, \tag{63}$$

and, making the substitution $U = \mathrm{d}C/\mathrm{d}z$, results in

$$\frac{\mathrm{d}C}{\mathrm{d}z} = U, \tag{64}$$
$$\frac{\mathrm{d}U}{\mathrm{d}z} = -\frac{vU}{D} - \frac{(K_i - K_g - \lambda_i + \lambda_g)A_1 C}{D}\left(1 - \frac{C}{A_1}\right)\left(C - A_2\right). \tag{65}$$

bioRxiv preprint doi: https://doi.org/10.1101/077743; this version posted September 27, 2016. The copyright holder for this preprint (which was not certified by peer review) is the author/funder. All rights reserved. No reuse allowed without permission.



Introducing a new variable $\overline{C} = C/A_1$ which, upon substitution into Equation (61), results in

$$\frac{\partial \overline{C}}{\partial t} = D\frac{\partial^2 \overline{C}}{\partial x^2} + (K_i - K_g - \lambda_i + \lambda_g)A_1^2\overline{C}(1-\overline{C})\left(\overline{C} - \overline{A}\right), \tag{66}$$

where

$$\overline{A} = \frac{A_2}{A_1} = \frac{2\lambda_i - \lambda - 2K_i + 2K_g + \sqrt{\lambda_g^2 + 4K_g(\lambda_i - \lambda_g - K_i + K_g)}}{2\lambda_i - \lambda - 2K_i + 2K_g - \sqrt{\lambda_g^2 + 4K_g(\lambda_i - \lambda_g - K_i + K_g)}}. \tag{67}$$

Equation (66) is a reaction-diffusion equation with Allee kinetics in terms of the scaled variable $\overline{C}$. Both the carrying capacity and Allee parameter are scaled by $A_1$, which influences the maximum population density as well as the threshold density required for positive growth. Following the analysis for Case 5, the minimum wave speed for Equation (66) with $\overline{A} < -1/2$ is $v^* = 2\sqrt{(\lambda_i - K_i)D}$. Interestingly, this implies that introducing grouped agent death at a rate that does not result in a population tending to extinction has no influence on the invasion speed of the population. Specifically, the condition for $A < -1/2$ in Case 5 corresponds to $3(\lambda_i - K_i) > \lambda_g$. It can be shown that, with $3(\lambda_i - K_i) > \lambda_g$, we require $3K_g < \lambda_g$ for $\overline{A} < -1/2$. This implies that there is a range of $K_g$ values that result in a travelling wave with a minimum wave speed that is independent of both $K_g$ and $\lambda_g$. Interestingly, this suggests that if a control is implemented that increases the death rate of grouped agents, there is a threshold value for the control to influence the invasion speed and the subsequent persistence of the population. Introducing a non-zero $K_g$ value for a parameter regime that results in the strong Allee effect with $K_g = 0$ never changes the type of Allee effect. Hence it is possible to go from a weak Allee effect to a reverse Allee effect by introducing a non-zero $K_g$ value. Non-zero $K_g$ values correspond to a decreased benefit for grouped agents, which explains why the source term, previously a weak Allee effect, becomes the reverse Allee effect, corresponding to inhibited growth at high density.

For the strong Allee effect, corresponding to $0 < A_2 < A_1 \leq 1$, the unique wave speed is $v = 2\sqrt{(K_i - K_g - \lambda_i + \lambda_g)D}(A_1/2 - A_2)$ [28]. This implies that for $A_2 > A_1/2$, $v < 0$ and $v > 0$ otherwise. Furthermore, the same wave speed applies for $-A_1/2 < A_2 < 0$ [28]. For both intervals, the minimum wave speed does depend on the $K_g$ value, and hence implementing any kind of partial eradication of the grouped agents will either reduce the speed of invasion or cause the extinction of the population.

bioRxiv preprint doi: https://doi.org/10.1101/077743; this version posted September 27, 2016. The copyright holder for this preprint (which was not certified by peer review) is the author/funder. All rights reserved. No reuse allowed without permission.



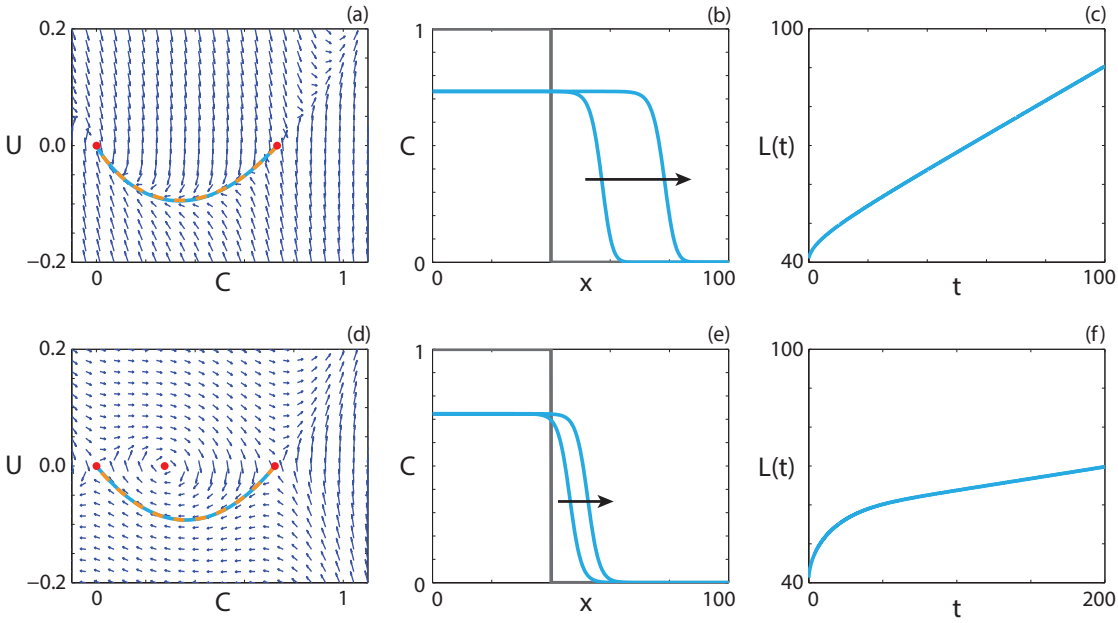


FIGURE 21. **Travelling wave behaviour for the (a)-(c) weak Allee effect and the (d)-(f) strong Allee effect with constant $F(C)$ (Case 7).** (a), (d) Phase plane for the system (64)-(65) with the numerical solution of Equations (61) (cyan, solid) and (63) (orange, dashed), in $(C, U)$ co-ordinates, superimposed. Red circles correspond to equilibrium points. (b), (e) Numerical solution of Equation (61) calculated at (b) $t = 50$ and $t = 100$, (e) $t = 100$ and $t = 200$. The grey lines indicate the initial condition and the arrows indicate the direction of increasing time. (c), (f) The time evolution of $L(t)$. All results are obtained with $\delta x = 0.1$, $\delta t = 0.01$, $\epsilon = 10^{-6}$, $P_d^g = 0.1$, (a)-(c) $P_m^i = 0.5$, $P_m^g = 0.5$, $P_p^i = 0.7$, $P_p^g = 0.4$, $P_d^i = 0.5$, $v = 0.44$, (d)-(f) $P_m^i = 1.0$, $P_m^g = 1.0$, $P_p^i = 0.7$, $P_p^g = 0.5$, $P_d^i = 0.8$, $v = 0.06$.

Travelling wave behaviour for the weak and strong Allee effect and constant $F(C)$ is shown in Figure 21. For both numerical solutions, calculated with $K_g = 0.1$, the carrying capacity is reduced by approximately 27%. With the exception of $K_g$, the parameters used to obtain the numerical solutions in Figures 21(a)-(c) are the same as in Figures 15(a)-(c) and we observe that, as expected, the wave speed is the same. This demonstrates that, while the carrying capacity is reduced, the population is able to invade vacant space at the same speed, even though a control measure for the grouped agents has been implemented. Results for the reverse Allee effect are presented in the Supplementary Material.

**Case 8: Different motility rates, different death rates.** Setting $P_m^i \neq P_m^g$ and $P_d^i \neq P_d^g \neq 0$ allows for significant flexibility in describing a combination of competitive and/or co-operative

bioRxiv preprint doi: https://doi.org/10.1101/077743; this version posted September 27, 2016. The copyright holder for this preprint (which was not certified by peer review) is the author/funder. All rights reserved. No reuse allowed without permission.



mechanisms, depending on the relevant motivation. In this case, Equation (1) can be expressed as

$$\frac{\partial C}{\partial t} = \frac{\partial}{\partial x}\left(F(C)\frac{\partial C}{\partial x}\right) + (K_i - K_g - \lambda_i + \lambda_g)A_1 C\left(1 - \frac{C}{A_1}\right)\left(C - A_2\right), \tag{68}$$

where $F(C) = D_i(1 - 4C + 3C^2) + D_g(4C - 3C^2)$. Note that, again, this simplification requires that $\lambda_g \geq 2(K_g + \sqrt{Kg(K_i - \lambda_i)})$ or $\lambda_i > K_i$, otherwise the population will tend to extinction. In travelling wave co-ordinates, Equation (68) is

$$v\frac{\mathrm{d}C}{\mathrm{d}z} + F(C)\frac{\mathrm{d}^2C}{\mathrm{d}z^2} + F'(C)\left(\frac{\mathrm{d}C}{\mathrm{d}z}\right)^2 + (K_i - K_g - \lambda_i + \lambda_g)A_1 C\left(1 - \frac{C}{A_1}\right)\left(C - A_2\right) = 0, \quad -\infty < z < \infty, \tag{69}$$

and, making the substitution $U = \mathrm{d}C/\mathrm{d}z$, it corresponds to

$$\frac{\mathrm{d}C}{\mathrm{d}z} = U, \tag{70}$$

$$\frac{\mathrm{d}U}{\mathrm{d}z} = -\frac{vU}{F(C)} - \frac{(D_i - D_g)(6C - 4)U^2}{F(C)} - \frac{(K_i - K_g - \lambda_i + \lambda_g)A_1 C}{F(C)}\left(1 - \frac{C}{A_1}\right)\left(C - A_2\right). \tag{71}$$

Introducing the variable $\overline{C} = C/A_1$, Equation (68) can be written as

$$\frac{\partial \overline{C}}{\partial t} = \frac{\partial}{\partial x}\left(F_A(\overline{C})\frac{\partial \overline{C}}{\partial x}\right) + (K_i - K_g - \lambda_i + \lambda_g)A_1^2\overline{C}(1 - \overline{C})(\overline{C} - \overline{A}), \tag{72}$$

where $F_A(\overline{C}) = F(A_1\overline{C}) = D_i(1 - 4A_1\overline{C}^2 + 3A_1^2\overline{C}^2) + D_g(4A_1\overline{C} - 3A_1^2\overline{C}^2)$. The transformed nonlinear diffusivity, $F_A(\overline{C})$, has the same characteristics as $F_s(\overline{C})$, presented in Figure 11, albeit in terms of the scaled Allee carrying capacity, $A_1$. Here we examine the five types of $F_A(\overline{C})$ for $A_1 \neq 1$.

*Sub-case 1: Strictly positive nonlinear diffusivity function.* For $F_A(\overline{C}) > 0$ on the interval $0 < \overline{C} \leq 1$, we follow the approach of Hadeler [42–44]. The integral condition for the wave speed to be positive,

$$\int_0^1 (K_i - K_g - \lambda_i + \lambda_g)A_1^2(D_i(1 - 4A_1\overline{C}^2 + 3A_1^2\overline{C}^2) + D_g(4A_1\overline{C} - 3A_1^2\overline{C}^2))\overline{C}(1 - \overline{C})(\overline{C} - \overline{A})\,\mathrm{d}\overline{C} > 0, \tag{73}$$

corresponds to

$$D_i(5 - 10\overline{A} + 6A_1^2 - 9A_1A_2 - 12A_1 + 20A_2) - D_g(6A_1^2 - 9A_1A_2 - 12A_1 + 20A_2) > 0. \tag{74}$$

bioRxiv preprint doi: https://doi.org/10.1101/077743; this version posted September 27, 2016. The copyright holder for this preprint (which was not certified by peer review) is the author/funder. All rights reserved. No reuse allowed without permission.



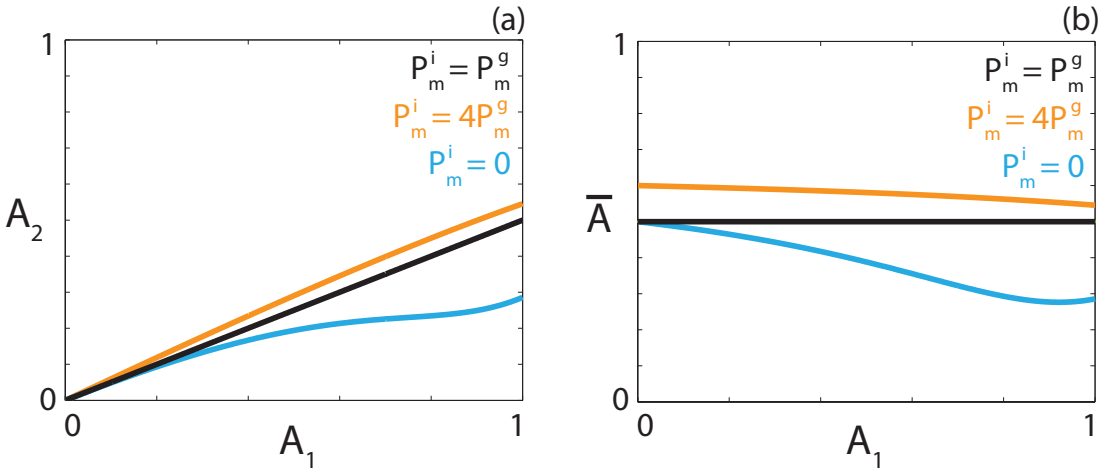


FIGURE 22. **Persistence threshold**. Persistence threshold as a function of the carrying capacity $A_1$, expressed as (a) an explicit value, and (b) a proportion of the carrying capacity for three different diffusivities, corresponding to $P^i_m = P^g_m$ (black), $P^i_m = 4P^g_m$ (orange) and $P^i_m = 0$ (cyan).

If $D_i = D_g$, then $\overline{A} > 1/2$ leads to $v < 0$. For the strong Allee effect, $A_1 > A_2 = \overline{A}A_1$, we can determine the threshold value for the persistence of the population, namely,

$$\overline{A} < \frac{5D_i + (D_i - D_g)(6A_1^2 - 12A_1)}{10D_i + (D_i - D_g)(9A_1^2 - 20A_1)}. \tag{75}$$

Considering the two limiting cases, where $D_i = 0$ and $D_i = 4D_g$, $\overline{A}$ takes on a value of $(6A_1^2 - 12A_1)/(9A_1^2 - 20A_1)$ and $(18A_1^2 - 36A_1 + 20)/(27A_1^2 - 60A_1 + 30)$, respectively. These values reduce to $6/11$ and $2/7$ in the case that $A_1 = 1$, as in Case 6.1. To illustrate how the threshold value changes with $A_1$, $P^i_m$ and $P^g_m$, Figure 22 shows the maximum $A_2$ and $\overline{A}$ values for three different $P^i_m$ and $P^g_m$ combinations. The $A_2$ value corresponds to the persistence threshold for a given $A_1$ value. The $\overline{A}$ value can be interpreted as the highest proportion of a given $A_1$ value that will result in the persistence of the population. For example, in Figure 22(a), we see that with $P^i_m = 0$ and $A_1 = 0.5$ we require $A_2 < 0.194$ for persistence. This corresponds to $\overline{A} < 0.388$.

Travelling wave behaviour for Equation (68) in a parameter regime corresponding to strictly positive $F_A(\overline{C})$ and the strong Allee effect is shown in Figures 23(a)-(c). This parameter regime leads to $A_1 = 0.723$ and $A_2 = 0.2764$, which is below the persistence threshold value of $A_2 = 0.315$ for this $P^i_m$ and $P^g_m$ combination, and hence the population persists.

bioRxiv preprint doi: https://doi.org/10.1101/077743; this version posted September 27, 2016. The copyright holder for this preprint (which was not certified by peer review) is the author/funder. All rights reserved. No reuse allowed without permission.



FIGURE 23. **Travelling wave behaviour for Equation** (68) **with various Allee effects and** $F_A(\overline{C})$. We consider the (a)-(c) scaled strong Allee effect with strictly positive $F_A(\overline{C})$ (Case 8.1), (d)-(f) scaled strong Allee effect with extinction-degenerate non-negative $F_A(\overline{C})$ (Case 8.2), (g)-(i) scaled strong Allee effect with positive-negative-positive $F_A(\overline{C})$ (Case 8.3) and, (j)-(l) scaled reverse Allee effect with capacity-degenerate $F_A(\overline{C})$ (Case 8.4). (a), (d), (g), (j) Phase plane for the system (70)-(71) with the numerical solution of Equations (68) (cyan, solid) and (69) (orange, dashed), in $(C, U)$ co-ordinates, superimposed. Red circles correspond to equilibrium points. (b), (e), (h), (k) Numerical solution of Equation (68) calculated at (b) $t = 250$ and $t = 500$, (e) $t = 200$ and $t = 400$, (h) $t = 250$ and $t = 500$, (k) $t = 100$ and $t = 200$. The grey lines indicate the initial condition and the arrows indicate the direction of increasing time. The inset corresponds to the area within the red dashed lines, and highlights the shock. (c), (f), (i), (l) The time evolution of $L(t)$. All results

bioRxiv preprint doi: https://doi.org/10.1101/077743; this version posted September 27, 2016. The copyright holder for this preprint (which was not certified by peer review) is the author/funder. All rights reserved. No reuse allowed without permission.



*Sub-case 2: Extinction-degenerate non-negative nonlinear diffusivity function.* For extinction-degenerate $F_A(\overline{C})$, $P_m^i = 0$. As such, the persistence threshold corresponds to $(6A_1^2 - 12A_1)/(9A_1^2 - 20A_1)$. For Case 6.2 we observe that sharp fronts for the strong Allee effect with a extinction-degenerate non-negative $F(C)$ only occur if $v > 0$. Hence for $\overline{A} < (6A_1^2 - 12A_1)/(9A_1^2 - 20A_1)$ Equation (68) should approach a sharp-fronted travelling wave solution with $v > 0$, and a smooth travelling solution with $v < 0$ otherwise. Results in Figures 23(d)-(f) show numerical solutions of Equation (68) with $A_1 = 0.723$ and $A_2 = 0.2764$, which satisfies the threshold for $v > 0$ and hence sharp-fronted travelling wave solutions exist. As expected, results in Figure 23(e) indicate that the solution of Equation (68) approaches a travelling wave with $v > 0$ and a sharp front near $C = 0$.

*Sub-case 3: Positive-negative-positive nonlinear diffusivity function.* For a positive-negative-positive $F_A(\overline{C})$, there are exactly two zeros at $C = \alpha$ and $C = \beta$. In Case 6.3 the strong Allee effect does not give rise to smooth travelling wave solutions, even with real-valued holes in the wall at $C = \alpha$ and $C = \beta$. However, interestingly, shock-fronted travelling wave solutions arise from the Heaviside initial condition. Again, we are unable to find numerical travelling wave solutions of Equation (68) in parameter regimes with real-valued holes in the wall. Shock-fronted travelling wave solutions of Equation (68) are given in Figures 23(g)-(i) where the observed wave speed is $v = 0.014 < 2\sqrt{\min\{F'(C)R(C)\}}$ on the interval $2A_1/3 < C < A_1$.

*Sub-case 4: Capacity-degenerate positive-negative nonlinear diffusivity function.* Capacity-degenerate positive-negative $F_A(\overline{C})$ requires $P_m^i = 0$ and, subsequently, $F_A(1) = 0$. Furthermore $F_A(\overline{C}) < 0$ for $\omega < C < S$. For Case 6.4 we found smooth travelling wave solutions for both the weak and reverse Allee effect with capacity-degenerate positive-negative $F(C)$ but could not obtain stable solutions for the strong Allee effect. As $F_A(\overline{C})$ is qualitatively similar to the $F(C)$ considered for Case 6.4 similar results are expected here.

Again, smooth travelling wave solutions of Equation (68) for both the weak (Figures 23(j)-(l)) and reverse (Supplementary Material) Allee effects are obtained. As for Case 6.4, we consider a variety of parameter regimes corresponding to the strong Allee effect with capacity-degenerate positive-negative $F_A(\overline{C})$, as well as a number of initial conditions, but are unable to find long time travelling wave-type solutions.

bioRxiv preprint doi: https://doi.org/10.1101/077743; this version posted September 27, 2016. The copyright holder for this preprint (which was not certified by peer review) is the author/funder. All rights reserved. No reuse allowed without permission.



*Sub-case 5: Positive-negative nonlinear diffusivity function.* For the case where $F_A(\overline{C})$ has exactly one zero on the interval $0 \leq \overline{C} \leq 1$ at $C = \omega$, Maini *et al.* [39] examine the existence of travelling wave solutions, and provide the necessary conditions for existence,

$$A_2 < \omega, \qquad v > 0, \qquad \int_0^{\omega} F(C)R(C)\,\mathrm{d}C > 0, \tag{76}$$

where $F(\omega) = 0$ and $0 < \omega < 1$. For the strong Allee effect in this parameter regime, the third part of Condition (76) corresponds to

$$\begin{aligned} &D_i(20(A_1 + A_2)\omega - 30A_1A_2\omega - 15\omega^2)+ \\ &(D_i - D_g)((84A_1 + 36A_2)\omega^3 - (45A_1A_2 + 60A_1 + 60A_2)\omega^2 - 30\omega^4 + 80A_1A_2\omega) > 0. \end{aligned} \tag{77}$$

As in Case 4.4, Equation (68) is equivalent to

$$\frac{\partial C}{\partial \hat{t}} = \frac{\partial^2 C}{\partial x^2} + (K_i - K_g - \lambda_i + \lambda_g)A_1F(C)C\left(1 - \frac{C}{A_1}\right)\left(C - A_2\right),\ \hat{t} \geq 0, \tag{78}$$

on the interval $0 \leq C < \omega$, and equivalent to

$$\frac{\partial C}{\partial \hat{t}} = \frac{\partial^2 C}{\partial x^2} + (K_i - K_g - \lambda_i + \lambda_g)A_1\hat{F}(C)(1 - C)\left(1 - \frac{1 - C}{A_1}\right)\left(1 - A_2 - C\right),\ \hat{t} \geq 0, \tag{79}$$

where $\hat{F}(C) = -F(1 - C)$, on the interval $\omega < C \leq A_1$. The final necessary and sufficient condition from Maini *et al.* [39] for the existence of travelling wave solutions is that the minimum wave speed for Equation (78), $v_1^*$, is greater than, or equal to, the minimum wave speed for Equation (79), $v_2^*$. On the interval $0 \leq C < \omega$, Equation (68) has a strictly positive $F_A(\overline{C})$, where $F_A(\overline{C}) \leq D_i$, and strong Allee kinetics. Hence, the minimum wave speed for Equation (78) has an upper bound, $v_1^* \leq \sqrt{2(\lambda_i - K_i)D_i}(1/2 - A_2)$. On the interval $\omega < C < A_1$ Equation (79) has a source term qualitatively similar to the Fisher-Kolmogorov equation and hence a lower bound for the minimum wave speed exists [39], $v_2^* \geq 2\sqrt{-F(A_1)(\lambda^2 + 4K_g(\lambda_i - \lambda_g - K_i + K_g))^{1/2}}$. For all parameter regimes considered that correspond to the strong Allee effect with positive-negative $F_A(\overline{C})$ we never observe a case where the upper bound for $v_1^*$ is higher than the lower bound for $v_2^*$ and hence the conditions required for travelling wave solutions are not met. As expected, numerical solutions of Equation (68) in these parameter regimes did not lead to travelling wave behaviour. For both the weak and the reverse Allee effect, we expect that solutions do exist as the source terms on both intervals are qualitatively equivalent to a Fisher source term.

bioRxiv preprint doi: https://doi.org/10.1101/077743; this version posted September 27, 2016. The copyright holder for this preprint (which was not certified by peer review) is the author/funder. All rights reserved. No reuse allowed without permission.



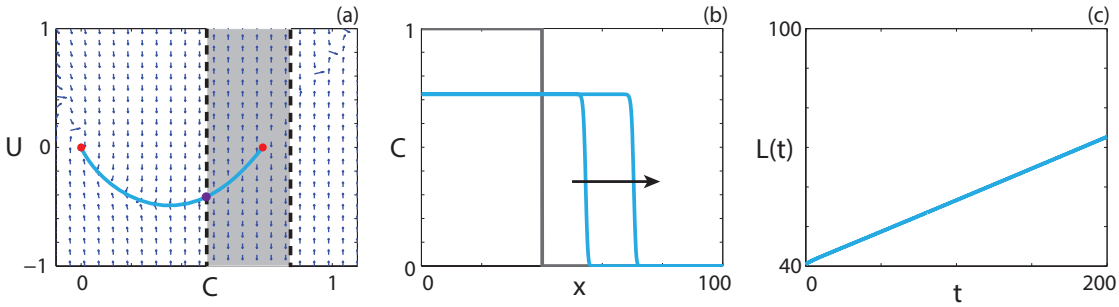


FIGURE 24. **Travelling wave behaviour for Equation** (68) **with the reverse Allee effect and positive-negative** $F_A(\overline{C})$ **(Case 8.5)**. (a) Phase plane for the system (70)-(71) with the numerical solution of Equation (68) (cyan, solid), in $(C, U)$ co-ordinates, superimposed. Red circles correspond to equilibrium points. (b) Numerical solution of Equation (68) calculated at $t = 100$ and $t = 200$. The grey lines indicate the initial condition and the arrows indicate the direction of increasing time. (c), (f) The time evolution of $L(t)$. All results are obtained with $\delta x = 0.1$, $\delta t = 0.01$, $\epsilon = 10^{-6}$, $P_d^g = 0.1$, $P_m^i = 0.025$, $P_m^g = 0.005$, $P_p^i = 0.7$, $P_p^g = 0.5$, $P_d^i = 0.2$, $P_d^g = 0.15$, $v = 0.16$.

Numerical solutions demonstrating the travelling wave behaviour of Equation (68) with positive-negative $F_A(\overline{C})$ and the reverse Allee effect are given in Figure 24.

## DISCUSSION

In this work we present a lattice-based discrete model of birth, death and movement. The model is an exclusion process, which means that it explicitly incorporates the effect of crowding by allowing no more than one agent per lattice site. A key feature of the model is that the rates at which birth, death and movement events occur depend on whether an agent is isolated or whether it is part of a group of agents. This means that the discrete model can be used to describe co-operative or competitive mechanisms, where there is a positive or negative benefit, respectively, of being part of the bulk population [8, 13–15]. These kind of mechanisms are thought to be relevant to many applications in cell biology [8, 12, 55, 56] and ecology [13–15]. By considering different combinations of parameters, the continuum limit PDE approximation of the discrete model leads to 22 different cases. These cases take the form of a reaction-diffusion equation with either Fisher kinetics, Allee kinetics, and a variety of density-dependent nonlinear diffusivity functions (Table 1). This approach also leads to a new kind of Allee effect, which we call the reverse Allee effect, where the growth rate is inhibited at high density. Although some

bioRxiv preprint doi: https://doi.org/10.1101/077743; this version posted September 27, 2016. The copyright holder for this preprint (which was not certified by peer review) is the author/funder. All rights reserved. No reuse allowed without permission.



of the PDEs that we consider have been investigated previously [36–41], they have never been linked together before in a single modelling framework.

For each class of PDE model, we examine properties of the long time travelling wave solutions. The travelling wave solutions of some of these PDEs have been analysed previously [15, 18–30]. However, some of the PDEs have been examined only in terms of the existence of travelling wave solutions [36–41] whereas we present numerical solutions here for the first time. One finding of our work is that PDE models with density-dependent nonlinear diffusivity functions that have regions of negative diffusivity require a sufficiently non-negative source term to support smooth travelling wave solutions. Furthermore, there appears to be a threshold proliferation value, depending on the rate of motility, that must be exceeded for travelling wave solutions to be observed numerically. However, we do not comment on the putative relationship between the parameters in the discrete model and the existence of travelling wave solutions in the continuum limit PDE. Interestingly, for the strong Allee effect, where the growth rate is negative for low agent densities [15], shock-fronted travelling wave solutions are obtained. Following arguments presented in [39], we show that smooth travelling wave solutions cannot be obtained for certain types of nonlinear diffusivity functions and the strong Allee effect. We describe how nonlinear diffusion can either hinder or promote the persistence of a population, and this balance depends on the relative motility rates of the isolated and grouped agents. Interestingly, the motility rates affect the persistence differently for different carrying capacities.

The six birth, death and motility rate parameters in the discrete model allow for the interpretation of the results in terms of whether individuals are part of, or isolated from, the bulk population. For example, a parameter regime corresponding to the strong Allee effect with constant diffusivity and no grouped agent death leads to the same travelling wave speed in the PDE description as a parameter regime corresponding to the strong Allee effect with constant diffusivity and a non-zero rate of grouped agent death, up to a threshold. This implies that a sufficiently strong intervention strategy aimed at grouped agents must be implemented if the goal of the intervention is to slow or halt the invasion of a population.

The work presented here suggests several avenues for future research. This work could be generalised by considering a two- or three–dimensional discrete process and deriving the continuum

bioRxiv preprint doi: https://doi.org/10.1101/077743; this version posted September 27, 2016. The copyright holder for this preprint (which was not certified by peer review) is the author/funder. All rights reserved. No reuse allowed without permission.



limit PDE descriptions in higher dimensions. This kind of higher-dimensional model might provide a more accurate description of real world observations where one-dimensional travelling wave solutions might not apply. In this work, numerical travelling wave solutions for each class of PDE are examined, but the formal stability of these travelling wave solutions is not considered. Another approach for analysing the discrete model would be to consider a coupled multispecies PDE model by accounting for the density of isolated agents and the density of grouped agents separately. This approach would lead to a system of two coupled PDEs instead of a single PDE for the total agent density. However, instead of working with coupled multispecies PDEs, we have taken the simplest and most fundamental approach of considering a single PDE description of the total population. In addition, a significant number of mechanisms could be implemented into the discrete model, such as cell-to-cell adhesion/repulsion [57, 58] or directed migration of isolated agents, such as chemotaxis [59]. We leave these extensions for future analysis.

## Methods

**Discrete model.** We consider a one-dimensional lattice-based random walk with $X$ sites and lattice spacing $\Delta$ [60]. Each site may be occupied by, at most, one agent [61–63]. The number of agents at time $t$ is $N(t)$. Agents attempt to undergo birth, death and movement events. During a birth event, an agent attempts to place a daughter agent at a randomly selected nearest-neighbour site. This event is successful provided that the selected site is vacant. During a death event, an agent is removed from the lattice. During a movement event, an agent attempts to move to a randomly selected nearest-neighbour site. This event is successful provided that the selected site is vacant. We distinguish between types of agents based on the number of occupied nearest-neighbour sites for each agent [64]. We refer to agents with zero occupied nearest-neighbour sites as *isolated agents*, and agents with one or two occupied nearest-neighbour sites as *grouped agents*. This approach allows us to specify different birth, death and movement rates for isolated and grouped agents.

Different parameter choices can be used to impose either co-operative or competitive mechanisms, where an increase in local agent density provides a positive or negative benefit, respectively. Specifically, in situations where the group motility or group proliferation rates are higher than the isolated motility or isolated proliferation rates, respectively, we interpret this choice of parameters as a model of co-operation. Similarly, in situations where the group motility or group

bioRxiv preprint doi: https://doi.org/10.1101/077743; this version posted September 27, 2016. The copyright holder for this preprint (which was not certified by peer review) is the author/funder. All rights reserved. No reuse allowed without permission.



proliferation rates are lower than the isolated motility or isolated proliferation rates, respectively, we interpret this as a model of competition.

During each time step of duration $\tau$, $N(t)$ agents are selected at random, one at a time, with replacement, and are given the opportunity to undergo a movement event. The constant probability that a selected agent attempts to undergo a movement event is $P_m^i$ for an isolated agent and $P_m^g$ for a grouped agent. We repeat this process for both birth and death events, with respective constant probabilities $P_p^i$ and $P_d^i$ for isolated agents and $P_p^g$ and $P_d^g$ for an agent within a group. At the end of each time step we update $N(t+\tau)$. To obtain the average agent density at each lattice site we perform $M$ identically-prepared realisations of the discrete model and average the binary lattice occupancy at each lattice site at each time step. In any single realisation of the discrete model we have $C_j = 1$ when site $j$ is occupied and $C_j = 0$ when site $j$ is vacant. To evaluate the average occupancy of any lattice site we consider an ensemble of $M$ identically-prepared realisations and calculate $\langle C_j \rangle = \sum_{m=1}^{M} C_j^m / M$.

**Mean-field description.** We derive a continuum limit PDE description of the discrete model [58, 63] by considering the change in occupancy of a lattice site $j$ during a single time step, and obtain

$$\begin{aligned}
\delta C_j =& \frac{P_m^i}{2}\Big[C_{j-1}(1-C_j)(1-C_{j-2}) + C_{j+1}(1-C_j)(1-C_{j+2}) - 2C_j(1-C_{j-1})(1-C_{j+1})\Big] \\
&+ \frac{P_m^g}{2}\Big[C_{j-1}(1-C_j) + C_{j+1}(1-C_j) - C_j(1-C_{j-1}) - C_j(1-C_{j+1})\Big] \\
&- \frac{P_m^g}{2}\Big[C_{j-1}(1-C_j)(1-C_{j-2}) + C_{j+1}(1-C_j)(1-C_{j+2}) - 2C_j(1-C_{j-1})(1-C_{j+1})\Big] \\
&+ \frac{P_p^i}{2}\Big[C_{j-1}(1-C_j)(1-C_{j-2}) + C_{j+1}(1-C_j)(1-C_{j+2})\Big] + \frac{P_p^g}{2}\Big[C_{j-1}(1-C_j) + C_{j+1}(1-C_j)\Big] \\
&- \frac{P_p^g}{2}\Big[C_{j-1}(1-C_j)(1-C_{j-2}) + C_{j+1}(1-C_j)(1-C_{j+2})\Big] \\
&- P_d^i\Big[C_j(1-C_{j-1})(1-C_{j+1})\Big] - P_d^g\Big[C_j\Big] + P_d^g\Big[C_j(1-C_{j-1})(1-C_{j+1})\Big]. \qquad (80)
\end{aligned}$$

Here, $C_j$ represents the probability that the site $j$ is occupied and, therefore, $1 - C_j$ represents the probability that the site is vacant [63]. Furthermore, as products of probabilities are interpreted as net transition probabilities, the usual assumption that the occupancy of lattice sites

bioRxiv preprint doi: https://doi.org/10.1101/077743; this version posted September 27, 2016. The copyright holder for this preprint (which was not certified by peer review) is the author/funder. All rights reserved. No reuse allowed without permission.



are independent is made [58, 61, 64–66].

Note that $C_j$ is the total occupancy of site $j$, that is, the sum of the occupancy of isolated agents and the occupancy of grouped agents at that site. We now interpret the terms on the right-hand side of Equation (80) in terms of the physical change in lattice occupancy. The positive terms proportional to $P_m^i$ correspond to isolated agents moving into site $j$, while the negative terms correspond to isolated agents moving out of site $j$. Each term consists of three factors. For the negative terms, these factors are the probability that site $j$ is occupied, and the probabilities that sites $j-1$ and $j+1$ are vacant. For the positive terms, the three factors are the probability that site $j \pm 1$ is occupied, and the probabilities that sites $j$ and $j \pm 2$ are vacant. The third factor is required to ensure that the term describes isolated agents. The positive/negative terms proportional to the first $P_m^g$ term on the right-hand side of Equation (80) correspond to grouped agents moving in/out of site $j$. These terms consist of two factors; the probability that the selected site is occupied and the probability that the target site is vacant. The second $P_m^g$ term ensures that the isolated agents are not counted twice. The remaining terms can be interpreted similarly; products of probabilities that specific sites are occupied or vacant that describe the change of occupancy of a site in response to a birth or death event.

To obtain a PDE description we divide Equation (80) by $\tau$ and consider $C_j$ as a continuous function, $C(x,t)$. Expanding $C(x,t)$ in a Taylor series around the point $x = j\Delta$, truncating terms of $\mathcal{O}(\Delta^3)$ [58, 63]. Taking the limit $\Delta \to 0$ and $\tau \to 0$ such that $\Delta^2/\tau$ is held constant [60, 63, 67] gives

$$\begin{aligned}\frac{\partial C}{\partial t} &= D_g \frac{\partial^2 C}{\partial x^2} + \Big(D_i - D_g\Big)\frac{\partial}{\partial x}\left(\Big(1 - 4C + 3C^2\Big)\frac{\partial C}{\partial x}\right) + \lambda_g C\Big(1 - C\Big) \\ &\quad + \Big(\lambda_i - \lambda_g\Big)C\Big(1 - C\Big)^2 - K_g C - \Big(K_i - K_g\Big)C\Big(1 - C\Big)^2, \end{aligned} \tag{81}$$

where

$$\begin{aligned} D_g = \lim_{\Delta,\tau\to 0}\frac{P_m^g \Delta^2}{2\tau}, \quad D_i = \lim_{\Delta,\tau\to 0}\frac{P_m^i \Delta^2}{2\tau}, \quad \lambda_g = \lim_{\tau\to 0}\frac{P_p^g}{\tau}, \quad \lambda_i = \lim_{\tau\to 0}\frac{P_p^i}{\tau}, \\ K_g = \lim_{\tau\to 0}\frac{P_d^g}{\tau}, \quad K_i = \lim_{\tau\to 0}\frac{P_d^i}{\tau}, \end{aligned} \tag{82}$$

with the further assumption that $P_p^i$, $P_p^g$, $P_d^i$, $P_d^g$ are $\mathcal{O}(\tau)$ [63]. The individual-level parameters are treated as being interchangeable with the continuum-level parameters as defined in (82). All

bioRxiv preprint doi: https://doi.org/10.1101/077743; this version posted September 27, 2016. The copyright holder for this preprint (which was not certified by peer review) is the author/funder. All rights reserved. No reuse allowed without permission.



implementations of the discrete model in this work have $\Delta = \tau = 1$.

It is convenient to write Equation (81) in conservation form

$$\frac{\partial C}{\partial t} = \frac{\partial}{\partial x}\left(F(C)\frac{\partial C}{\partial x}\right) + R(C), \tag{83}$$

where

$$F(C) = D_i(1 - 4C + 3C^2) + D_g(4C - 3C^2), \tag{84}$$

is the nonlinear diffusivity function, and

$$R(C) = \lambda_g C(1 - C) + (\lambda_i - \lambda_g - K_i + K_g)C(1 - C)^2 - K_g C, \tag{85}$$

is the source/sink term.

**Numerical techniques.** Here we describe the techniques used to obtain numerical solutions of Equation (1), the corresponding ODE in travelling wave co-ordinates, and to generate the phase planes in $(C, U)$ co-ordinates.

*Partial differential equations.* To obtain numerical solutions of Equation (1), we first spatially discretise Equation (1) onto a grid with uniform grid spacing $\delta x$ by approximating the spatial derivatives with a central finite difference approximation. A backward Euler approximation with constant time steps of duration $\delta t$ is used to approximate the temporal derivative. The resulting system of nonlinear algebraic equations is solved using Picard iteration with absolute convergence tolerance $\epsilon$. The resulting system of tridiagonal algebraic equations is solved using the Thomas algorithm [68]. All results presented correspond to sufficiently small choices of $\delta x$, $\delta t$ and $\epsilon$ so that the numerical solutions are grid independent. In all cases consider zero-flux boundary conditions are considered, and the finite domain is sufficiently large such that the numerical solution of Equation (1) does not interact with the boundaries on the time scale of the numerical simulations. All numerical solutions correspond to a Heaviside initial condition with $C = 1$ for $x \leq X_0$, and $C = 0$ otherwise.

*Ordinary differential equations.* The second order ODEs in the travelling wave co-ordinates are solved using Matlab's `ode45` routine [69]. This routine implements an adaptive Runge-Kutta method with relative error tolerance of $10^{-3}$ and an absolute error tolerance of $10^{-6}$ [69]. For travelling wave ODEs that contain a singularity are not solved numerically. Therefore, for these

bioRxiv preprint doi: https://doi.org/10.1101/077743; this version posted September 27, 2016. The copyright holder for this preprint (which was not certified by peer review) is the author/funder. All rights reserved. No reuse allowed without permission.



singular problems we obtain only the numerical solution of the PDE and present this solution in the transformed $(C, U)$ travelling wave co-ordinate system.

*Phase planes.* To generate phase planes we substitute $U = \mathrm{d}C/\mathrm{d}z$ into the second order travelling wave ODE to obtain a system of two first-order ODEs. The phase plane is constructed by considering 22 equally-spaced values of $C$ and 22 equally spaced values of $U$ to calculate both $\mathrm{d}C/\mathrm{d}z$ and $\mathrm{d}U/\mathrm{d}z$ at all $22 \times 22 = 484$ pairs of $(C, U)$ values. In each phase plane the same 22 equally spaced values of $C$ on the interval $0 \leq C \leq 1$ are considered. However, depending on the steepness of the waveform, we choose a different interval of $U$ to construct the phase plane, and this choice is made to accommodate the heteroclinic orbit. The phase planes are constructed using Matlab's `quiver` function. The location of the equilibrium points, where $\mathrm{d}C/\mathrm{d}z = \mathrm{d}U/\mathrm{d}z = 0$ are superimposed. Furthermore, in many cases the expression for $\mathrm{d}U/\mathrm{d}z$ has a rational form, $\mathrm{d}U/\mathrm{d}z = G(C, U)/H(C, U)$. In these cases both the wall of singularities $(H(C, U) = 0)$ and the locations of the holes in the wall $(H(C, U) = G(U, C) = 0)$ are also superimposed.

## Acknowledgements

This work is supported by the Australian Research Council (DP140100249, FT130100148).

## Author contributions

STJ, REB, DLSM and MJS conceived the experiments, STJ performed the experiments, STJ, REB, DLSM and MJS analysed the results, STJ and MJS wrote the manuscript. All authors read and approved the final version of the manuscript.

## Additional information

**Competing financial interests.** The authors declare no competing financial interests.

## References

[1] Alvord Jr, E. C. & Shaw, C. M. *Neoplasms affecting the nervous system of the elderly* (Oxford University Press, 1991).

[2] Clavero, M. & García-Berthou, E. Invasive species are a leading cause of animal extinctions. *Trends in Ecology and Evolution* **20**, 110–110 (2005).

bioRxiv preprint doi: https://doi.org/10.1101/077743; this version posted September 27, 2016. The copyright holder for this preprint (which was not certified by peer review) is the author/funder. All rights reserved. No reuse allowed without permission.



[3] Gabriely, G. *et al.* MicroRNA 21 promotes glioma invasion by targeting matrix metalloproteinase regulators. *Molecular and Cellular Biology* **28**, 5369–5380 (2008).

[4] Gerlee, P. & Nelander, S. The impact of phenotypic switching on glioblastoma growth and invasion. *PLOS Computational Biology* **8**, e1002556 (2012).

[5] Gerlee, P. & Nelander, S. Travelling wave analysis of a mathematical model of glioblastoma growth. *Mathematical Biosciences* **276**, 75–81 (2016).

[6] Johnston, S. T., Simpson, M. J. & McElwain, D. L. S. How much information can be obtained from tracking the position of the leading edge in a scratch assay? *Journal of The Royal Society Interface* **11**, 20140325 (2014).

[7] Martin, P. Wound healing – aiming for perfect skin regeneration. *Science* **276**, 75–81 (1997).

[8] Poujade, M. *et al.* Collective migration of an epithelial monolayer in response to a model wound. *Proceedings of the National Academy of Sciences* **104**, 15988–15993 (2007).

[9] Sherratt, J. A., Lewis, M. A. & Fowler, A. C. Ecological chaos in the wake of invasion. *Proceedings of the National Academy of Sciences* **92**, 2524–2528 (1995).

[10] Swanson, K. R., Bridge, C., Murray, J. D. & Alvord, E. C. Virtual and real brain tumors: using mathematical modeling to quantify glioma growth and invasion. *Journal of the Neurological Sciences* **216**, 1–10 (2003).

[11] Townsend, C. R. Invasion biology and ecological impacts of brown trout *salmo trutta* in New Zealand. *Biological Conservation* **78**, 13–22 (1996).

[12] Axelrod, R., Axelrod, D. E. & Pienta, K. J. Evolution of cooperation among tumor cells. *Proceedings of the National Academy of Sciences* **103**, 13474–13479 (2006).

[13] Courchamp, F., Clutton-Brock, T. & Grenfell, B. Inverse density dependence and the Allee effect. *Trends in Ecology and Evolution* **14**, 405–410 (1999).

[14] Godin, J. G. J. Antipredator function of shoaling in teleost fishes: a selective review. *Le Naturaliste Canadien* **113**, 241–250 (1986).

[15] Taylor, C. M. & Hastings, A. Allee effects in biological invasions. *Ecology Letters* **8**, 895–908 (2005).

[16] Semmens, B. X. *et al.* Quasi-extinction risk and population targets for the Eastern, migratory population of monarch butterflies (danaus plexippus). *Scientific Reports* **6**, 23265 (2016).

[17] Wang, J. *et al.* A framework for the assessment of the spatial and temporal patterns of threatened coastal delphinids. *Scientific Reports* **6**, 19883 (2016).

[18] Ablowitz, M. J. & Zeppetella, A. Explicit solutions of Fisher's equation for a special wave speed. *Bulletin of Mathematical Biology* **41**, 835–840 (1979).

[19] Aronson, D. G. & Weinberger, H. F. Multidimensional nonlinear diffusion arising in population genetics. *Advances in Mathematics* **30**, 33–76 (1978).

[20] Bramson, M. Convergence of solutions of the Kolmogorov equation to travelling waves **44**, 285 (1983).

[21] Canosa, J. On a nonlinear diffusion equation describing population growth. *IBM Journal of Research and Development* **17**, 307–313 (1973).

[22] Fife, P. C. & McLeod, J. B. The approach of solutions of nonlinear diffusion equations to travelling front solutions. *Archive for Rational Mechanics and Analysis* **65**, 335–361 (1977).

bioRxiv preprint doi: https://doi.org/10.1101/077743; this version posted September 27, 2016. The copyright holder for this preprint (which was not certified by peer review) is the author/funder. All rights reserved. No reuse allowed without permission.



[23] Fife, P. C. Long time behavior of solutions of bistable nonlinear diffusion equations. *Archive for Rational Mechanics and Analysis* **70**, 31–36 (1979).

[24] Fisher, R. A. The wave of advance of advantageous genes. *Annals of Eugenics* **7**, 355–369 (1937).

[25] Hadeler, K. P. & Rothe, F. Travelling fronts in nonlinear diffusion equations. *Journal of Mathematical Biology* **2**, 251–263 (1975).

[26] Keitt, T. H., Lewis, M. A. & Holt, R. D. Allee effects, invasion pinning, and species borders. *The American Naturalist* **157**, 203–216 (2001).

[27] Kolmogorov, A. N., Petrovsky, I. G. & Piskunov, N. S. Étude de léquation de la diffusion avec croissance de la quantité de matiere et son application un probleme biologique. *Moscow University Mathematics Bulletin* **1**, 1–25 (1937).

[28] Lewis, M. A. & Kareiva, P. Allee dynamics and the spread of invading organisms. *Theoretical Population Biology* **43**, 141–158 (1993).

[29] Murray, J. D. *Mathematical Biology I: An Introduction* (Springer, New York, 2002).

[30] Rothe, F. Convergence to pushed fronts. *Journal of Mathematics* **11**, 617–634 (1981).

[31] Johnston, S. T., Shah, E. T., Chopin, L. K., McElwain, D. L. S. & Simpson, M. J. Estimating cell diffusivity and cell proliferation rate by interpreting IncuCyte ZOOM assay data using the Fisher-Kolmogorov model. *BMC Systems Biology* **9**, 38 (2015).

[32] Maini, P. K., McElwain, D. L. S. & Leavesley, D. Travelling waves in a wound healing assay. *Applied Mathematics Letters* **17**, 575–580 (2004).

[33] Maini, P. K., McElwain, D. L. S. & Leavesley, D. I. Traveling wave model to interpret a wound-healing cell migration assay for human peritoneal mesothelial cells. *Tissue Engineering* **10**, 475–482 (2004).

[34] Sherratt, J. A. & Murray, J. D. Models of epidermal wound healing. *Proceedings of the Royal Society of London B: Biological Sciences* **241**, 29–36 (1990).

[35] Ito, H. *et al.* Evolution of periodicity in periodical cicadas. *Scientific Reports* **5**, 14094 (2015).

[36] Ferracuti, L., Marcelli, C. & Papalini, F. Travelling waves in some reaction-diffusion-aggregation models. *Advances in Dynamical Systems and Applications* **4**, 19–33 (2009).

[37] Kuzmin, M. & Ruggerini, S. Front propagation in diffusion-aggregation models with bi-stable reaction. *Discrete and Continuous Dynamical Systems: Series B* **16**, 819–833 (2011).

[38] Maini, P. K., Malaguti, L., Marcelli, C. & Matucci, S. Diffusion-aggregation processes with mono-stable reaction terms. *Discrete and Continuous Dynamical Systems: Series B* **6**, 1175–1189 (2006).

[39] Maini, P. K., Malaguti, L., Marcelli, C. & Matucci, S. Aggregative movement and front propagation for bi-stable population models. *Mathematical Models and Methods in Applied Sciences* **17**, 1351–1368 (2007).

[40] Sánchez-Garduño, F. & Maini, P. K. Existence and uniqueness of a sharp travelling wave in degenerate non-linear diffusion Fisher-KPP equations. *Journal of Mathematical Biology* **33**, 163–192 (1994).

[41] Sánchez-Garduño, F. & Maini, P. K. Travelling wave phenomena in non-linear diffusion degenerate Nagumo equations. *Journal of Mathematical Biology* **35**, 713–728 (1997).

[42] Hadeler, K. P. Travelling fronts and free boundary value problems. In *Numerical Treatment of Free Boundary Value Problems*, 90–107 (Springer, 1982).

bioRxiv preprint doi: https://doi.org/10.1101/077743; this version posted September 27, 2016. The copyright holder for this preprint (which was not certified by peer review) is the author/funder. All rights reserved. No reuse allowed without permission.



[43] Hadeler, K. P. Free boundary problems in biological models. *Free boundary problems: Theory and applications* **2**, 664–671 (1983).

[44] Hadeler, K. P. Traveling fronts in parabolic and hyperbolic equations. In *Dynamical Systems*, 154–164 (Springer, 1987).

[45] Malaguti, L. & Marcelli, C. Sharp profiles in degenerate and doubly degenerate Fisher-KPP equations. *Journal of Differential Equations* **195**, 471–496 (2003).

[46] Sherratt, J. A. & Marchant, B. P. Nonsharp travelling wave fronts in the Fisher equation with degenerate nonlinear diffusion. *Applied Mathematics Letters* **9**, 33–38 (1996).

[47] Sherratt, J. A. On the form of smooth-front travelling waves in a reaction-diffusion equation with degenerate nonlinear diffusion. *Mathematical Modelling of Natural Phenomena* **5**, 64–79 (2010).

[48] Padrón, V. Effect of aggregation on population recovery modeled by a forward-backward pseudoparabolic equation. *Transactions of the American Mathematical Society* **356**, 2739–2756 (2004).

[49] Malaguti, L., Marcelli, C. & Matucci, S. Front propagation in bistable reaction-diffusion-advection equations. *Advances in Differential Equations* **9**, 1143–1166 (2004).

[50] Landman, K. A. & White, L. R. Terraced spreading of nanofilms under a nonmonotonic disjoining pressure. *Physics of Fluids* **23**, 012004 (2011).

[51] Witelski, T. P. Shocks in nonlinear diffusion. *Applied Mathematics Letters* **8**, 27–32 (1995).

[52] Pettet, G. J., McElwain, D. L. S. & Norbury, J. Lotka-volterra equations with chemotaxis: Walls, barriers and travelling waves. *Mathematical Medicine and Biology* **17**, 395–413 (2000).

[53] Wechselberger, M. & Pettet, G. J. Folds, canards and shocks in advection–reaction–diffusion models. *Nonlinearity* **23**, 1949 (2010).

[54] Forbes, L. K. & Derrick, W. A combustion wave of permanent form in a compressible gas. *The ANZIAM Journal* **43**, 35–58 (2001).

[55] Korolev, K. S., Xavier, J. B. & Gore, J. Turning ecology and evolution against cancer. *Nature Reviews Cancer* **14**, 371–380 (2014).

[56] Sewalt, L., Harley, K., van Heijster, P. & Balasuriya, S. Influences of Allee effects in the spreading of malignant tumours. *Journal of Theoretical Biology* **394**, 77–92 (2016).

[57] Anguige, K. & Schmeiser, C. A one-dimensional model of cell diffusion and aggregation, incorporating volume filling and cell-to-cell adhesion. *Journal of Mathematical Biology* **58**, 395–427 (2009).

[58] Johnston, S. T., Simpson, M. J. & Baker, R. E. Mean-field descriptions of collective migration with strong adhesion. *Physical Review E* **85**, 051922 (2012).

[59] Keller, E. F. & Segel, L. A. Model for chemotaxis. *Journal of Theoretical Biology* **30**, 225–234 (1971).

[60] Codling, E. A., Plank, M. J. & Benhamou, S. Random walk models in biology. *Journal of the Royal Society Interface* **5**, 813–834 (2008).

[61] Baker, R. E. & Simpson, M. J. Correcting mean-field approximations for birth-death-movement processes. *Physical Review E* **82**, 041905 (2010).

[62] Chowdhury, D., Schadschneider, A. & Nishinari, K. Physics of transport and traffic phenomena in biology: from molecular motors and cells to organisms. *Physics of Life Reviews* **2**, 318–352 (2005).

bioRxiv preprint doi: https://doi.org/10.1101/077743; this version posted September 27, 2016. The copyright holder for this preprint (which was not certified by peer review) is the author/funder. All rights reserved. No reuse allowed without permission.



[63] Simpson, M. J., Landman, K. A. & Hughes, B. D. Cell invasion with proliferation mechanisms motivated by time-lapse data. *Physica A: Statistical Mechanics and its Applications* **389**, 3779–3790 (2010).

[64] Johnston, S. T., Baker, R. E. & Simpson, M. J. Filling the gaps: A robust description of adhesive birth-death-movement processes. *Physical Review E* **93**, 042413 (2016).

[65] Simpson, M. J. & Baker, R. E. Corrected mean-field models for spatially dependent advection-diffusion-reaction phenomena. *Physical Review E* **83**, 051922 (2011).

[66] Johnston, S. T., Simpson, M. J. & Baker, R. E. Modelling the movement of interacting cell populations: a moment dynamics approach. *Journal of Theoretical Biology* **370**, 81–92 (2015).

[67] Hughes, B. D. *Random Walks and Random Environments*, vol. 1 (Clarendon Press; Oxford University Press, 1995).

[68] Press, W. H. *Numerical Recipes 3rd Edition: The Art of Scientific Computing* (Cambridge University Press, 2007).

[69] Shampine, L. F. & Reichelt, M. W. The Matlab ODE suite. *SIAM Journal on Scientific Computing* **18**, 1–22 (1997).